Joining Carbon Fiber and Aluminum with Ultrasonic Additive Manufacturing

Undergraduate Honors Thesis

Presented in Partial Fulfillment of the Requirements for

Graduation with Distiction at

The Ohio State University

By

M. Bryant Gingerich,

* * * * *

The Ohio State University

2014

Master's Examination Committee:

Dr. Marcelo J. Dapino, Adviser

Dr. Anthony Luscher

Approved by

Adviser

Undergraduate Program in

Mechanical Engineering

ABSTRACT

Due to increasing emphasis on vehicle lightweighting to increase fuel efficiency, integration of carbon fiber composites with metal structures is necessary. Current adhesive and mechanical fastening methods used for joining carbon fiber composites to metals are not ideal due to cost, corrosion issues, stress concentrations, poor peel strength, and composite delamination. Consequently, new joining techniques are needed for increasing the use of carbon fiber composites. In this research project a novel method of creating joints between carbon fiber and 6061-T6 aluminum was explored by using ultrasonic additive manufacturing (UAM). The UAM process was used to embed dry carbon fibers within an aluminum matrix, creating a mechanical joint between the two materials. The joints were then wet with epoxy and tested in tension. The epoxy acted as a load distributing agent by bonding the embedded fibers to each other. Pullout strength results suggest that the UAM joining process can be used to create joints with strength exceeding that of the carbon fiber being joined. Further developments showed that full bidirectional carbon fiber fabric can be embedded within an aluminum matrix. SEM and optical imaging of joint cross sections showed that the joint strength comes from a mechanical interlocking between the carbon fibers and the aluminum. UAM joining of carbon fiber to aluminum shows promise and with further development may prove superior to current industry standard joining techniques.

ACKNOWLEDGMENTS

I would like to thank a number of individuals who have helped me immensely with this undergraduate research project. First of all, I would like to thank my adviser, Professor Dapino for allowing me to be a part of his exciting and groundbreaking research. I am grateful for his insightful guidance throughout the project as well as his financial support. I would like to thank Adam J. Hehr, who was a mentor to me throughout this project. Adam's encouragement, support, and willingness to help can not be overstated. I would also like to thank other UAM researchers Paul Wolcott and Matt Scheidt for their advice, support, and friendship. Special thanks to Prof. Luscher for his willingness to serve on my examination committee. Thanks to John Larson for help with literature and to Justin Scheidler for his assistance with the formatting of this document. This acknowledgment would not be complete without recognizing the team from Fabrisonic, Mark Norfolk and Cameron Benedict, who have faithfully kept the UAM machine running - often coming to the rescue on very short notice.

Outside of lab, I have an amazing network of family and friends who have supported me in my decision to study engineering. To my friends, thanks for providing an outlet for activities outside of lab. To my mentors: Phil, Noah, Willard, Brian, and Rod, thank you for your prayers and words of wisdom. To my grandparents: Marvin

and Betty, Lloyd, thank you for your love, prayers, and financial support. Your impact on my life is more than you can know. To my family, thanks for love, laughter, and encouragement. Mom and dad, thanks for your constant guidance through this transition season of my life. I thank God for you daily.

- Soli Dei Gloria -

TABLE OF CONTENTS

Page

Abstract ii

Acknowledgments iii

List of Tables vii

List of Figures viii

Chapters:

1. Introduction 1

    1.1 Literature Survey 1
        1.1.1 Background 1
        1.1.2 Current Joining Methods 3
        1.1.3 Joining of Aluminum to CFRP by Ultrasonic Welding . . . 5
        1.1.4 Ultrasonic Additive Manufacturing 9
    1.2 Objectives 17

2. Embedding Carbon Fiber within 6061-T6 Aluminum 19

    2.1 Initial Embedding Attempts 19
        2.1.1 Joint Preparation and Results 19
        2.1.2 UAM Parameters 22
        2.1.3 Discussion 22
    2.2 Embedding of Single CF Bundles With Channels 24
        2.2.1 Joint Preparation and Results 24
        2.2.2 UAM Process Parameters 25
        2.2.3 Discussion 25
    2.3 Mechanical Testing 26

2.3.1 Testing Design and Setup 26
2.3.2 Dry Carbon Fiber Pullout Results 28
2.3.3 Epoxy Wetted Carbon Fiber Pullout Results 29
2.3.4 Analysis and Discussion 31
2.4 Embedding of Half Density CF Bidirectional Textile 33
2.4.1 Joint Design and Preparation 33
2.4.2 UAM Process Parameters 34
2.4.3 Results 34
2.4.4 Joint Integrated into CF Structure 35
2.5 Embedding of Full Density CF Bidirectional Textile 36
2.5.1 Joint Design and Preparation 37
2.5.2 UAM Process Parameters 38
2.5.3 Results 39

3. Manufacturing Control 43

3.1 Downforce Stability 43
3.1.1 Force Profile Before and After Controller Modification . . . 43
3.1.2 Effect of Welding Speed 47
3.1.3 Discussion 49
3.2 Substrate Compliance Model 50
3.2.1 Material Properties and Joint Geometry 51
3.2.2 Modeling Technique 53
3.2.3 Results and Discussion 60

4. Design for Multi-Ply CF to Aluminum Tensile Test Specimen 62

4.1 Initial Stacking Attempt 62
4.2 Proposed Joint Design 65

5. Concluding Remarks 68

5.1 Summary 68
5.2 Future Work 70

Bibliography 73

LIST OF TABLES

Table		Page
2.1	UAM parameters used for single bundle embedding.	22
2.2	Initial UAM parameters used embedding bidirectonal CF textile. . .	38
2.3	Final UAM parameters used embedding bidirectional CF textile. . .	39
3.1	Joint geometry constants and material properties used in compliance model.	52
3.2	Compliance model stiffness values.	60

LIST OF FIGURES

Figure		Page
1.1	Lap shear response comparison between adhesive joint and adhesive/welded joint [11].	5
1.2	Ultrasonic welding parameters and other factors influencing joint strength [7].	6
1.3	Orientation of ultrasonic metal and plastic welding [7].	7
1.4	Contrasting the single lap strength of U. P. W. with that of U. M. W [5].	8
1.5	UAM system tools for ultrasonic welding and milling operations. (Courtesy of Fabrisonic)	10
1.6	Basic principles of UAM (courtesy of Fabrisonic).	12
1.7	VHP UAM system used by the Smart Materials and Structures Laboratory at The Ohio State University.	14
1.8	Schematic of a peel test for testing UAM layer bond strength. [19]	16
1.9	Push pin test for testing UAM welded layer bonding.	16
1.10	Shear and tensile mechanical testing of UAM welded builds [15].	17
2.1	Unidirectional CF fabric embedding attempt with fibers parallel to tape feed. (a) Before welding, (b) After welding attempt.	20
2.2	Cross sectional diagram explaining roll crushing of fibers when embedding fibers oriented perpendicular to the weld oscillations without channels.	21

2.3 Embedding of single bundles oriented perpendicular to the tape feed. (a) Before embedding. (b) After first tape layer was welded over fibers. 21

2.4 Embedding of a single CF bundle spread out and oriented perpendicular to tape feed. (a) Before embedding. (b) After welding one layer of tape over fibers. 22

2.5 SEM images of embedded spread out carbon fiber bundle. 23

2.6 Embedding single CF bundles with channels to house the fiber bundles. (a) Bundles laid into channels prior to embedding. (b) Embedded CF bundles. 24

2.7 SEM images of embedded CF bundle in channel. 25

2.8 Schematic showing pullout test specimen construction. 27

2.9 In house load frame with pullout fixture for embedded fiber pullout strength test. 28

2.10 (a) Pullout strength test specimens before testing. (b) Specimens after failure. 29

2.11 (a) Pullout strength test specimens with epoxy before testing. (b) Specimens after failure (right). 30

2.12 Pullout strength of epoxy impregnated joints compared with the strength of dry joints. 31

2.13 Three different failure modes seen in CF - Al joints wetted with epoxy. (a) Specimen E3, complete pullout from joint; (b) Specimen E4, failure in the fiber gauge length - no joint failure; (c) Specimen E5, brittle failure near the front edge of joint. 32

2.14 (a) CF textile preparation with horizontal fibers removed in the weld region. (b) Channels cut to house the CF bundles. (c) CF bundles secured in place prior to welding. (d) First layer of aluminum tape welded over CF textile. 35

2.15 Progression of removing CF to aluminum joint from baseplate and integrating into CF structure. 36

2.16 (a) Channels geometry used to embed bidirectional CF. (b) Fibers placed into channels prior to embedding. 38

2.17 Tape tearing after first embedding layer. 40

2.18 First aluminum tape layer welded over bidirectional CF textile with no tape tearing. 40

2.19 Comparison of embedded CF from different locations of the joint. The light gray speckles between the carbon fibers in the closeup images is penetrated aluminum. (a) Embedded CF perpendicular to weld direction. (b) Closeup of (a). (c) Embedded CF parallel to weld direction. (d) Closeup of (c). 42

3.1 Downforce profile during the length of a even weld before and after controller gain adjustments. 45

3.2 Downforce profile during the first layer of foil embedding bidirectional CF fabric before and after controller gain adjustments. 46

3.3 The average of standard deviation over individual channels during the first layer of welded foil over the channels. 47

3.4 Effect of weld speed on force profile while welding first layer of aluminum tape over bidirectional CF fabric. 49

3.5 Cross section of embedded bidirectional CF fabric with very poor inter-laminate bonding over the embedded fibers. 51

3.6 Schematic showing compliance model dimensions and annotating the three sections analyzed in Section 3.2.2. 53

3.7 Region 1 of the compliance model. 55

3.8 Region 2 of the compliance model. 57

3.9 Region 3 of the compliance model. 59

4.1 Poor bonding with LWD of near zero in the region above embedded CF. 64

4.2 Delamination due to poor bonding over embedded channels. Delamination occurred during a machining operation. 65

4.3 Proposed joint with increased tape thickness and reduced channel depth. 66

CHAPTER 1

INTRODUCTION

1.1 Literature Survey

1.1.1 Background

With fuel efficiency becoming an increasing concern, the design and manufacture of lightweight vehicles has been on the rise. This is the case in the automotive industry as well as the aerospace industry. To achieve effective weight reduction, composite materials are starting to be used in many structural applications. In high performance situations the use of carbon fiber reinforced polymers (CFRP) is becoming increasing common. In October of 2011, the Boeing 787 Dreamliner commercial aircraft made its debut. Half of the Dreamliners weight is made from carbon fiber composites reducing the weight of the aircraft by 20% when compared to more conventional aluminum designs [13]. Such weight reduction is beneficial to fuel economy, reducing operating costs as well as leaving a smaller carbon footprint. According to the aerospace consultancy firm, AeroStrategy LLC, in 2008 the aerospace industry accounted for nearly 60% of the carbon fiber produced. This is mainly due to the large quantities of carbon fiber used by aircraft giants Boeing and Airbus [25].

While there is certainly motivation for the automotive industry to adopt the use of carbon fiber, it has been slower to embrace this lightweighting technology. For automotive applications, reducing vehicle weight by 100 kg on the average vehicle corresponds to a 0.3-0.4 liter per 100 km reduction in fuel consumption [17]. Currently carbon fiber use in automobiles is mostly limited to high end sports cars and race cars. One of the main reasons for the slow adoption process of carbon fiber by the automotive industry is cost. Carbon fiber costs approximately 20 USD/kg, this should be compared to the price of steel which is only 1 USD/kg. Despite the cost, automotive manufacturer BMW has already adopted CFRP into their mass produced i3 series [23]. BMW expects to reduce the cost of a carbon fiber frame down to the level of aluminum by year 2020 [23]. They have made a huge step toward vehicle lightweighting and other auto manufacturers will follow. The use of carbon fiber in the automotive industry is increasing due to carbon fiber cost reduction and recent advances in carbon fiber manufacturing techniques.

One of main advances in carbon fiber technology is in resin transfer molding (RTM) techniques. Resin transfer molding involves a reinforcement mat and low viscosity resin which is injected under pressure. First a dry unimpregnated carbon fiber pre-shaped reinforcement is prepared into the preform which is the skeleton of the actual part to be created. The preform is paired with a matching die mold. After the mold is closed the resin is injected under pressure. Heat is then applied to activate the curing process. The part can be removed from the mold as soon as it develops sufficient strength for handling. [17] Japanese textile manufacturer and carbon fiber products supplier, Toray Industries, has developed a carbon fiber processing method that will make mass production of lightweight, carbon fiber vehicles possible. This

process marries proprietary resin transfer molding techniques with enhanced resin infiltration and hardening technologies. This improved process has been used to shorten the molding cycle from 160 minutes to 10 minutes. Studies have shown that these CFRP parts are 1.5 times safer in a collision than steel parts. This program to develop CFRP parts for automotive use is backed by the Japanese Government. [25]

Recent innovations in resin transfer molding has made producing large and complex shapes with good laminate surface quality possible. The process also enables integration of ribs, cores and inserts. While the RTM process allows integration with some load attachments and secondary structures, the requirement to join to other load attachment points and secondary structures is unavoidable [17]. These structural components could include metallic space frames or secondary structures including seat mountings and suspension systems. Composite materials are much more complex than metallic ones in the way they support loadings. Metallic materials are nearly homogenous and can dissipate local stress concentrations due to plasticity. Composites on the other hand exhibit material anisotropy, poor interlaminar strength and lack local stress relief [17]. Developing joining techniques for composites is challenging, but is necessary to tackle for enabling robust integration of CFRP structures into automotive and aerospace products.

1.1.2 Current Joining Methods

The most common method of joining metal components in the automotive industry is spot welding. For metal to metal joints, this method has been used to create high strength joining and can be integrated into efficient, highly automated processes. However, traditional spot welds cannot be used with CFRP to metal joining [12]. As a

result, joining techniques including adhesives, mechanical fasteners, or a combination of the two have been used [17]. The primary method of joining composites to metals is by high-strength adhesive joining. Adhesive joining is favored over mechanical fasteners such as bolts and rivets because these methods produce point-source loadings which requires thicker, heavier material [30]. Adhesive joining also offers inherent galvanic corrosion protection when joining materials such as carbon fiber to metals [30]. While adhesive joining has a number of important positive points, it is not without flaws.

The primary shortcoming of adhesive joining is inherently weak peal strength [8]. In practice, bonded structures are exposed to a combination of different loadings. These include tensile, compressive, shear, cleavage and peel stresses. Engineers usually design some form of lab shear joint for use with adhesives. These joints are not ideal structurally because under load both shear and peel stresses are activated [2]. There is little that can be done to reduce the amount of induced peel stress in simple lap joints. Additionally, surface finish does not have a substantial effect on peel strength as it does in tensile strength [27]. As a result, optimizing the surface finish is not a viable solution to reducing peel failure.

Hybrid joints have been developed which feature adhesive joining aided by welded steel clamping [11]. The strength and toughness of this hybrid joint is compared with plain adhesive joining in Figure 1.1. Hybrid joints are an improvement over purely adhesive joints because they reduce delamination and peel failure. Consequently, the strength of welded/adhesive joints is slightly greater than adhesive joints and the toughness is greatly improved. Another positive point of hybrid joints is that the

joint can be clamped together via the welding while the adhesive is curing [30]. This allows for a more streamlined manufacturing process.

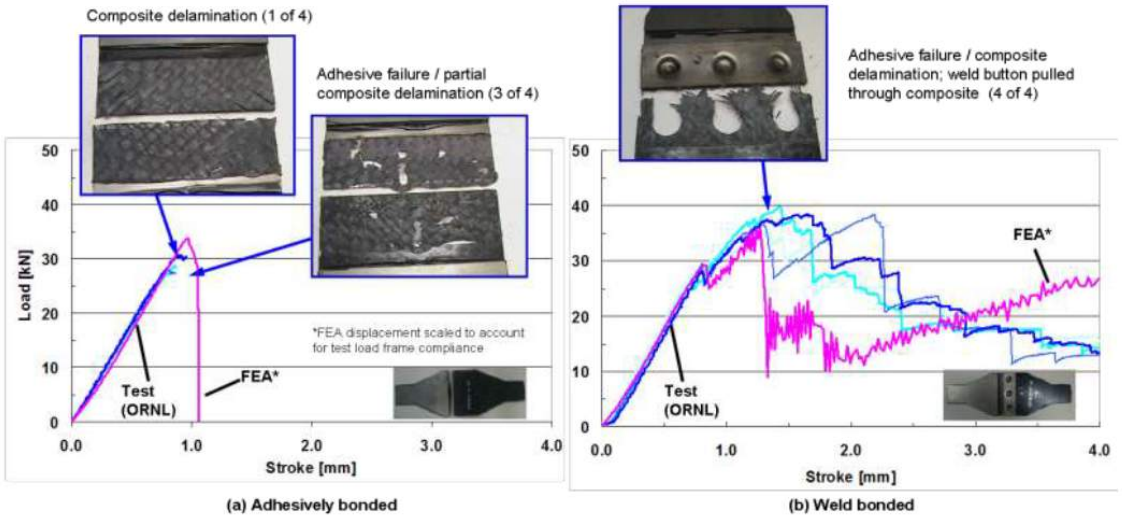

Figure 1.1: Lap shear response comparison between adhesive joint and adhesive/welded joint [11].

Other recently developed joining methods for CFRP to metals include friction spot joining [3], metal to metal foam to composite joining [31], cold metal transfer pin techniques [26], and ultrasonic welding [4]. These joining techniques will not be discussed in detail with the exception of ultrasonic welding, since the process is similar to the ultrasonic additive manufacturing process used in this research project.

1.1.3 Joining of Aluminum to CFRP by Ultrasonic Welding

Ultrasonic welding is a solid state welding technique where the joining occurs as the result of static pressure coupled with ultrasonic oscillations directed from a weld head (often called the sonotrode) into the two joining structures. When compared to fusion

welding or brazing, ultrasonic welding is marked by low energy input. This results in a joining process that is characterized by low maximum temperatures. Ultrasonic welding is particularly well suited to welding of thin foils of metal or thin sheets to thicker sheets. Dissimilar metals can also be welded with high power ultrasonic welders. [5]

The primary welding parameters used in ultrasonic welding include oscillation amplitude, welding force exerted on the joint, welding energy, and workpiece temperature. It is possible to create robust welded joints between unique materials combinations by properly adjusting the welding parameters for the application. In addition to welding parameters, the joining surface conditions and part geometry can also play large factors in the quality of ultrasonically welded joints as illustrated in Figure 1.2.

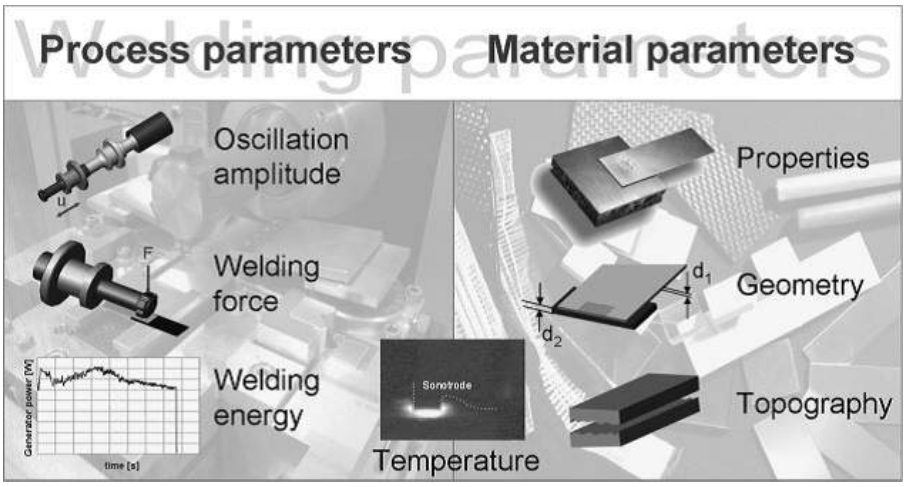

Figure 1.2: Ultrasonic welding parameters and other factors influencing joint strength [7].

There are two primary types of ultrasonic welders. These are defined by their sonotrode oscillation orientations. Ultrasonic metal welders have transducers which induce oscillations parallel to the joining surfaces. Ultrasonic metal welding (UMW) is well suited for joining of metals. Conversely, ultrasonic plastic welding (UPW) features sonotrode oscillations perpendicular to the joining surfaces. Ultrasonic plastic welding has traditionally been used for the welding of polymers. [5]

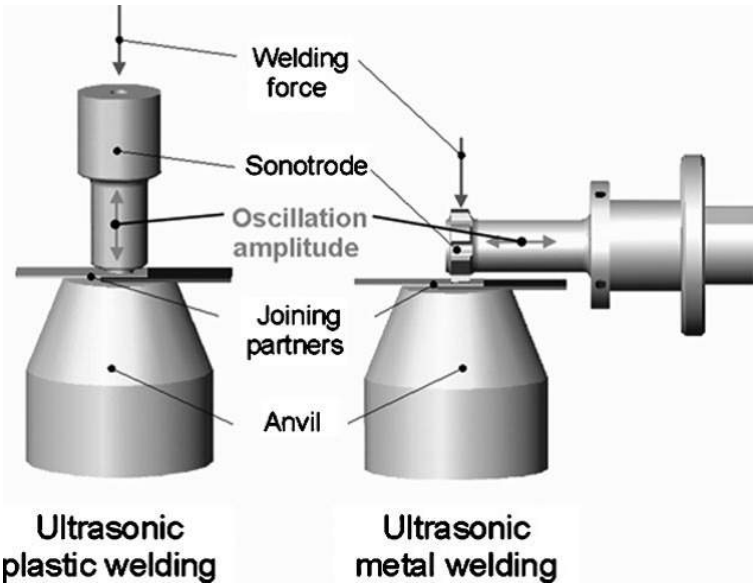

Figure 1.3: Orientation of ultrasonic metal and plastic welding [7].

Balle et al. [5] showed that ultrasonic metal welding is more effective in joining carbon fiber reinforced polymers to metals than ultrasonic plastic welding. The CFRP chosen for welding in this study had a thermoplastic matrix (PA66). The reason for using a thermoplastic matrix was to allow energy from the ultrasonic welder to push the matrix between the carbon fibers and the metal interface aside. This matrix choice is important, because carbon fiber composites with epoxy as the matrix cannot be

welded [30]. Using UMW with the PA66 matrix resulted in direct mechanical joining between the metal and carbon fibers. When ultrasonic plastic welding was used, it was much less effective in pushing the matrix aside, resulting in a intermediate layer of thermoplastic matrix between the fibers and metal [5].

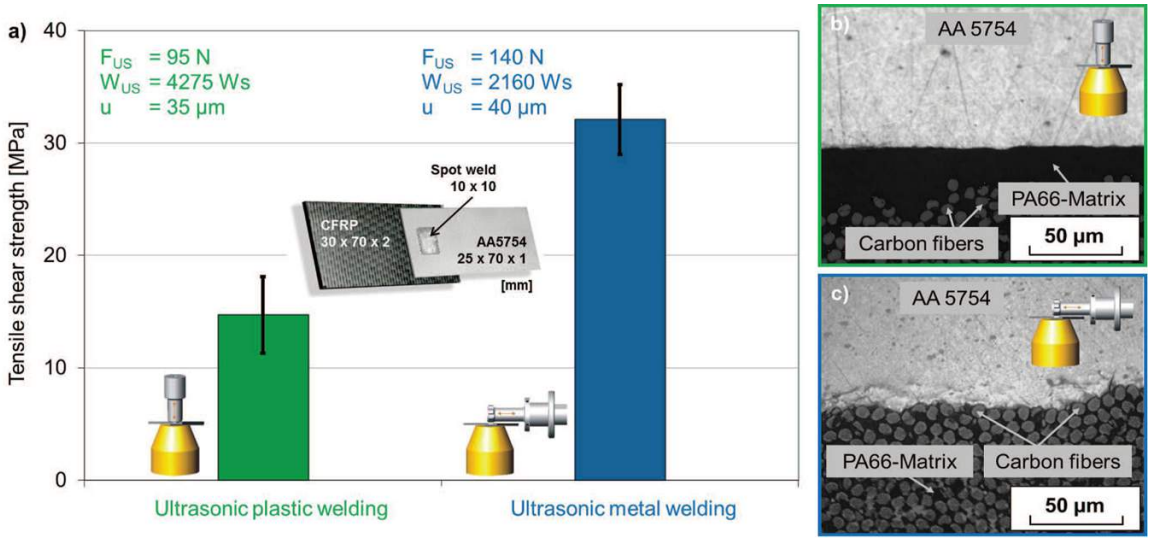

Figure 1.4: Contrasting the single lap strength of U. P. W. with that of U. M. W [5].

Balle et al. had excellent results with joining aluminum to CFRP with a PA66 matrix. Further improvements of this joining method were achieved by making surface finish modifications including acid etching and corundum-blasting of the aluminum joining member. Using this pre-welding surface treatment, the joint strength was increased from 30MPa to nearly 50MPa [6]. However, the main shortcoming of ultrasonic welding of CFRP to aluminum is that it requires a thermoplastic matrix. Thermoplastics are not typically used along with resin transfer molding. Instead, thermoset plastics are used including polyester, vinyl ester, and epoxy [29]. Structurally speaking, epoxy

is more resistant to deformation when exposed to heat than thermoplastics. While UMW can be used to effectively join CFRP to aluminum, this joining method is not ideal for automotive manufacturing because of its incompatibility with the RTM process.

1.1.4 Ultrasonic Additive Manufacturing

Ultrasonic Additive Manufacturing (UAM) which is also referred to as Ultrasonic Consolidation (UC) is a manufacturing process that uses additive and subtractive steps to create unique, three-dimensional structures from metal foils. The UAM method has been used to create multi-functional structures with unique internal geometries and internal integration of wiring, electronics, and fiber optics [24]. UAM is performed from a machine tool which is used in a Computer Numeric Control (CNC) manufacturing center. UAM was first commercially introduced by Solidica Inc. [24]. The Solidica Formation machine incorporated a metal welding head (sonotrode) equipped with an automated tape feed, a standard 3-axis milling head, and software to automatically control tool paths for both the weld head and milling head [24]. Pictured in Figure 1.5, the weld head is treated by the CNC machine as a tool and is used to additively join metal foils to create desired builds.

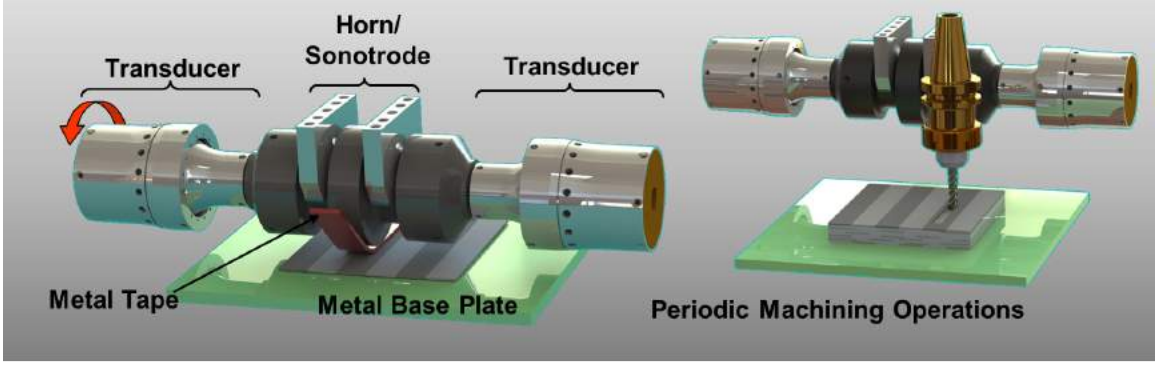

Figure 1.5: UAM system tools for ultrasonic welding and milling operations. (Courtesy of Fabrisonic)

An important characteristic of UAM is that the temperature at the weld interface during the joining process typically does not exceed 30%-50% of the melting temperature of the metal [20]. This unique low temperature joining creates possibilities for embedding temperature sensitive fibers and materials with little to no damage. Another unique aspect of UAM is that highly localized plastic flow is possible around embedded structures [22]. This capability coupled with the low temperatures of welding make UAM an excellent method for embedding many types of materials within a metal matrix.

The UAM process has been used successfully with a variety of metals including Al, Ni, Ti, Ag, Cu, Ta and others as well as joining of many combinations of dissimilar metals [21]. Regardless of material, the same principles in UAM are at work to create joining between the metal layers. Figure 1.6 illustrates the basic principles of UAM. In the process, a rotating sonotrode travels over the length of the weld. A thin metal tape is laid under the sonotrode as it travels over the work piece. The base structure is secured by the mill table which is often equipped with a vacuum chuck. Transducers

create a 20 kHz signal which is amplified by boosters and drives the sonotrode at the amplitude specified by the operator transverse to the foil layup direction. As the sonotrode moves over the work piece, it is pushed into the two joining materials by the weld tool at a specified loading. The surface of the sonotrode is textured in a manner such that it grips the metal tape forcing the two adjacent surfaces to move relative to each other at 20 kHz and at a specified amplitude. The combinations of normal and oscillatory forces result in a scrubbing action causing dynamic interfacial stresses at the foilbase interface. These stresses produce high plastic deformation of surface asperities which effectively break up the oxide layer leading to metallurgical bonding between the metal layers [24]. Once one layer of metal foil has been welded to the base structure, additional layers can be welded adjacent to the original foil if necessary to construct the desired structure. Further layers can be welded over the first layer of foils until the desired build thickness is achieved. During the construction process, the UAMs milling tool can be used to remove necessary material from the structure. This machining capability makes complex internal geometries and embedding dissimilar materials possible. After all necessary foils have been welded, further machining can be done to complete the part.

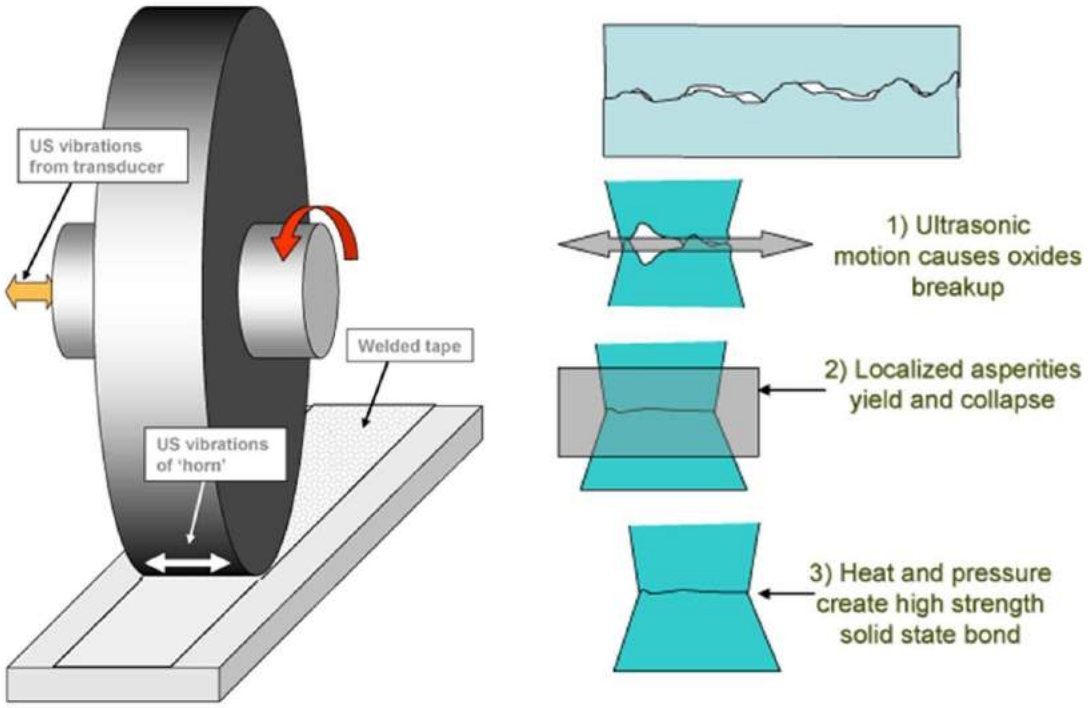

Figure 1.6: Basic principles of UAM (courtesy of Fabrisonic).

Much like ultrasonic metal welding, the UAM process has a number of parameters which affect the quality of the additive foil process. The parameters can be altered per specific application to render robust joining between the foils and/or embedded structures. The typical parameters include: normal force, sonotrode amplitude, weld speed, baseplate temperature, and sonotrode roughness. The normal force is applied by the welding tool and is monitored by a load cell within the horn assembly. Sonotrode amplitude is the peak to peak movement of the horn driven by the transducers. The amplitude can easily be altered by the operator. The frequency of the oscillations, however, is not easily changed as it is limited by the sonotrode geometry and power supply. The frequency is usually near 20 kHz for UAM applications. Weld

speed is the rate at which the sonotrode roles over the metal foils during the welding process. Many UAM systems are equipped with the option of a heated baseplate. The temperature is controlled by a heating element in the anvil of the UAM system. Lastly, the sonotrode will have a specified surface roughness. The roughness of the horn provides friction with the foil to be joined. There are different levels of roughness that can be used depending on the application.

UAM systems used today include first generation models capable of power up to 1kW to more recent very high power (VHP) UAM systems that can provide 9.5kW of power. The VHP-UAM systems were developed at Edison Welding Institute (EWI) located in Columbus, OH. VHP-UAM systems have increased capabilities for greater normal force and oscillation amplitude. This improvement over the original lower powered systems allows for superior joining with aluminum and steel and makes bonding high strength metals such as titanium and stainless steel possible. Figure 1.7 shows a VHP-UAM system used by the Smart Materials and Structures Laboratory at The Ohio State University.

Figure 1.7: VHP UAM system used by the Smart Materials and Structures Laboratory at The Ohio State University.

Since UAM is an emerging process, there is ongoing work being done in examining the fundamentals of the process. Current research includes optimizing techniques and parameters to achieve strong bonding between foil layers. This research includes characterizing methods and parameters for a variety of materials. A common method of evaluating the quality of a weld is to calculate the Linear Weld Density (LWD). Linear Weld Density is the percentage of bonded region along a foil to foil interface divided by the length of the entire interface. LWD is defined in Equation (1.1).

$$\%LWD = \frac{\text{Bonded interface length}}{\text{Total interface length}} \times 100. \tag{1.1}$$

While LWD has been widely used to characterize the bond strength of UAM made parts, the method does not always accurately represent the bond strength between

foil layers. The bonding strength of UAM joints is more complex than simply looking at area of the joint that seems to be bonded. Additionally, calculating LWD requires optical methods which can often lead to high levels of error. To better understand foil to foil strength, delamination tests can be used. Typical delamination tests include peel tests and push pin tests. Peel strength tests are conducted by peeling welded foils apart and measuring the force required to peel the layers apart [10] as pictured in Figure 1.8. A major limitation of peel testing is that its results are difficult to understand and compare with other testing methods unless the entire layer can be removed from the substrate. This limits peel testing to layers with poor bond strength [33]. Push pin tests are conducted by pushing a pin into the surface of a prepared test specimen as show in Figure 1.9. During testing to failure, load and displacement and recorded for analysis. Push pin testing is often preferable to peel testing because of its simpler test setup and compatibility with strong bonding between layers. The push pin method can also be combined with finite element analysis to establish correlations between the push pin results and the ultimate strength of the bonded layers [33].

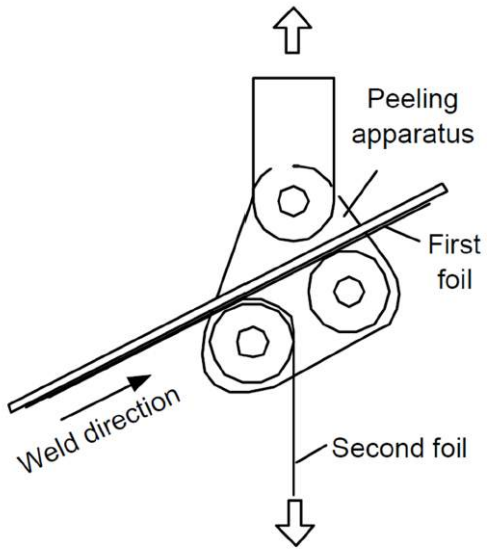

Figure 1.8: Schematic of a peel test for testing UAM layer bond strength. [19]

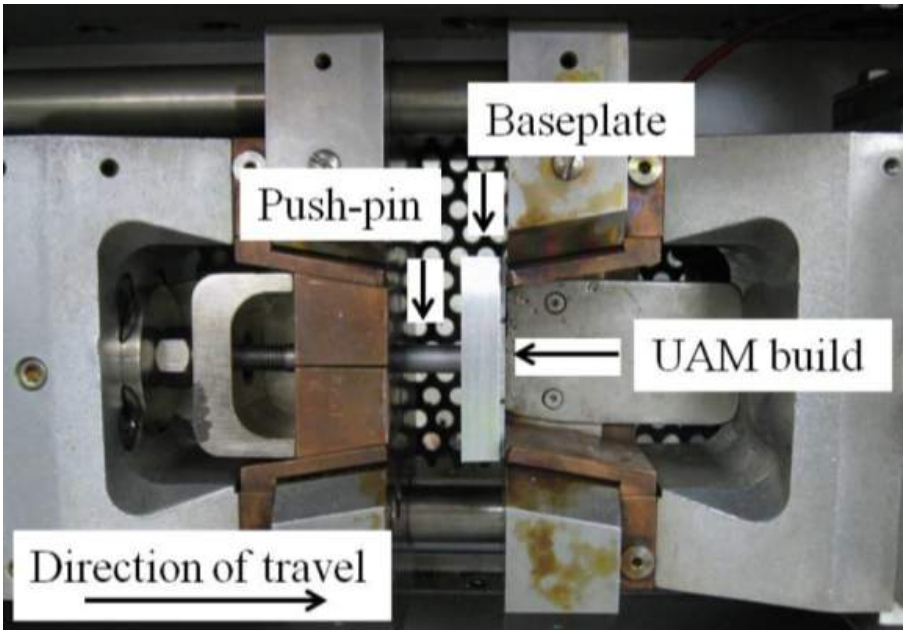

Figure 1.9: Push pin test for testing UAM welded layer bonding.

Another common mechanical testing method for determining layer bond strength is traditional shear and tensile testing. Force and displacement data is recorded to determine the bond strength. For tensile testing, one requirement of this method is the strength of the adhesive media used to join the gripping structure to the test specimen must exceed the strength of the bonded layers. This requirement can be avoided by creating an entire dog-bone test specimen of bonded layers as seen in Figure 1.10 [15].

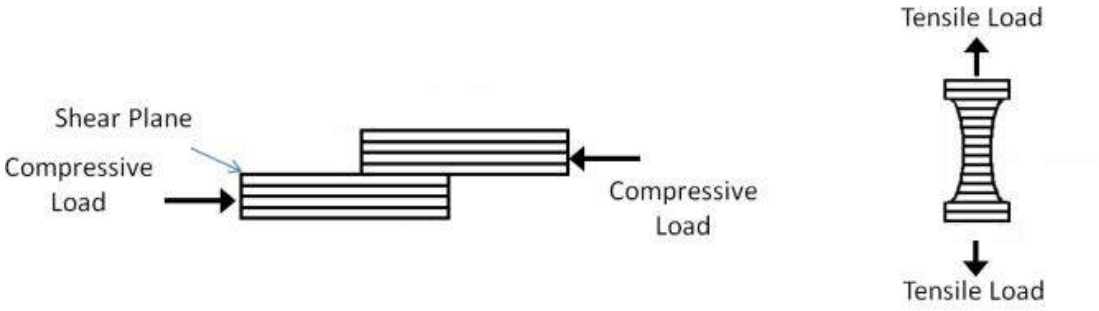

Figure 1.10: Shear and tensile mechanical testing of UAM welded builds [15].

1.2 Objectives

As discussed in Section 1.1.4, the UAM process can be used to embed dissimilar materials within a metal matrix. Given the unsatisfactory capabilities of current joining methods used for integrating CFRP structures with metal structures, there is a need for alternative joining techniques in the automotive and aerospace industries. It is possible that the UAM process could be used to create superior joints. This could have a large impact on industry as more manufacturers begin to implement carbon fiber composites into their products. The purpose of this project is explore

embedding of CF by the UAM process, starting with simple build geometries and progressing to more complex joints.

The UAM process can be used with a number of different metals including steel, aluminum, and titanium. If automotive manufacturers were to use the UAM process to create CF to metal joints, the metal of choice would be steel in most cases. To date, however, the vast majority of UAM research has been done using aluminum. It therefore follows that this project focuses on joining carbon fiber with aluminum. Future work will include transferring aluminum to CF joining technology to other metals such as steel.

In addition to exploring build designs for embedding CF into aluminum, an important part if this project is to examine the quality and strength of the joints created by microscopy and mechanical testing. Cross sectioning embedded carbon fibers is crucial to understanding the joint mechanisms and improving the joining process. Mechanical testing must be performed to understand whether or not creating carbon fiber to aluminum joints using the UAM process is an improvement over current joining methods.

The final goal of this project is to develop a method which can be used to embed multiple layers of bidirectional CF fabric in a single build. This would simulate how the joint would be built if adopted by industry. In future work, this design would be used to create a test specimen which would be tested along side an adhesive lap joint to determine if the UAM CF to aluminum joint is a strength improvement over the currently used adhesive joints.

CHAPTER 2

EMBEDDING CARBON FIBER WITHIN 6061-T6 ALUMINUM

2.1 Initial Embedding Attempts

2.1.1 Joint Preparation and Results

Prior to this project, little work had been done on embedding CF between layers of aluminum. Furthermore, there is no literature on consolidating carbon fibers with the UAM process. Consequently, reasoning behind initial joint configurations was determined primarily by following joint patterns used for embedding other fiber-like materials such as NiTi fibers [14].

The first attempt at embedding fiber bundles was made by laying a section of unidirectional fabric parallel with the aluminum tape feed. A small detachable base of 6061-T6 aluminum was used as the base substrate. This base was attached to a vacuum plate mounted to the UAM system table. The results of this consolidation attempt were poor. As seen in Figure 2.1, the embedding attempt failed due to severe crushing of the fibers. The crushed fibers pasted graphite over the intended weld area, preventing bonding between the layers of aluminum tape.

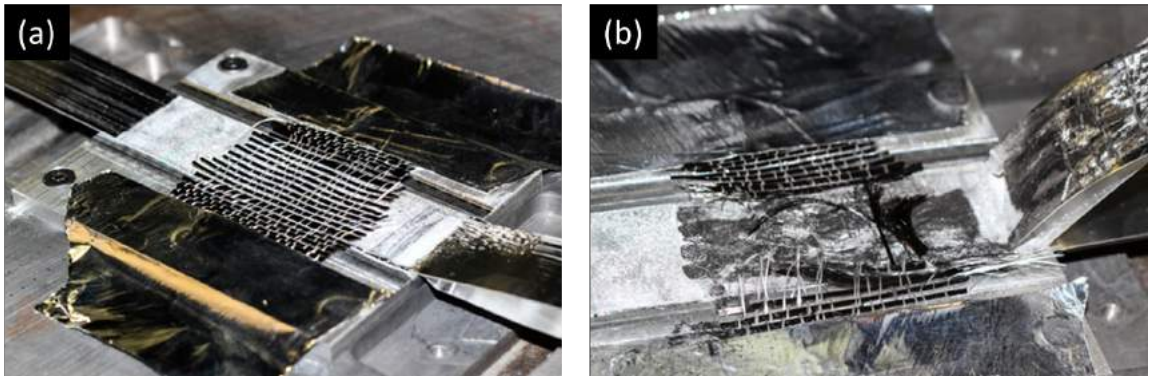

Figure 2.1: Unidirectional CF fabric embedding attempt with fibers parallel to tape feed. (a) Before welding, (b) After welding attempt.

It was theorized that fiber crushing from the embedding process would be reduced by orienting the CF bundles perpendicular to tape feed. Figure 2.2 illustrates how orienting the fibers parallel to the tape feed (perpendicular to the weld head oscillations) results in fiber crushing. The diameter of the each carbon fiber is approximately 5 μm while the welding oscillations required to properly bond the aluminum tape with the substrate is 32 μm. The welding force combined with osculations with amplitude far greater than the diameters of the fibers results in the fibers rolling back and forth against each other, reducing them to a graphite paste.

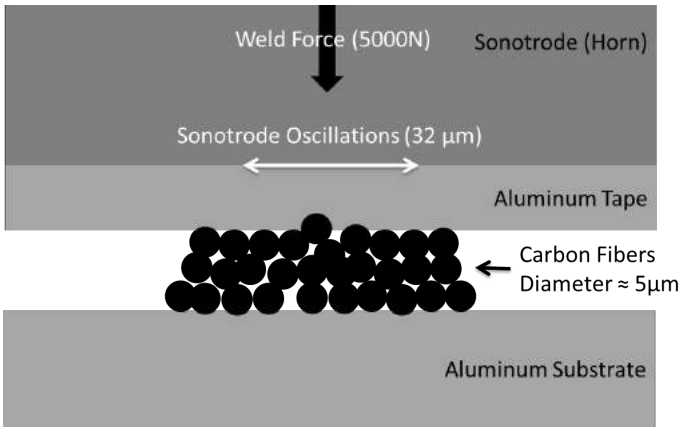

Figure 2.2: Cross sectional diagram explaining roll crushing of fibers when embedding fibers oriented perpendicular to the weld oscillations without channels.

Carbon fiber embedding attempts were far more successful when orienting the fibers perpendicular to the tape feed. Single bundles were embedded as seen in Figures 2.3 and 2.4. In each of these cases, successful consolidation was achieved. However, the fibers were either cut or severely damaged at the tape edge. Continuous fibers are necessary to create joints between CF structures and UAM welded parts.

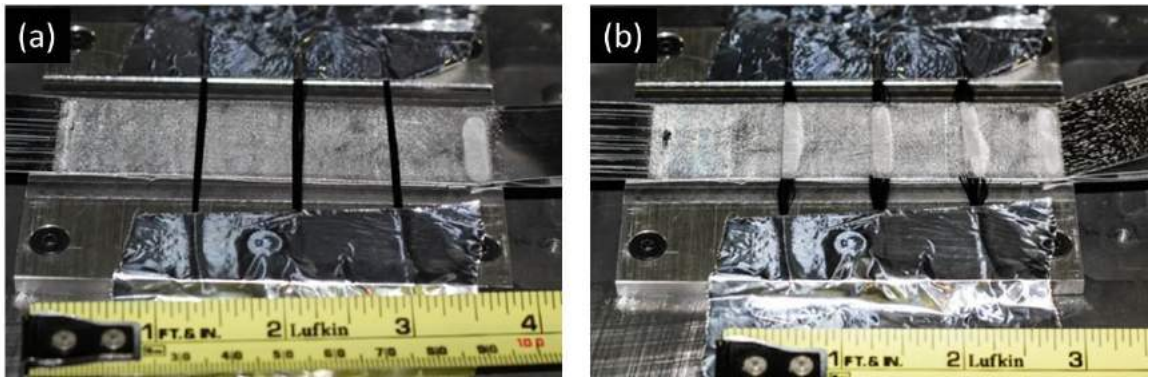

Figure 2.3: Embedding of single bundles oriented perpendicular to the tape feed. (a) Before embedding. (b) After first tape layer was welded over fibers.

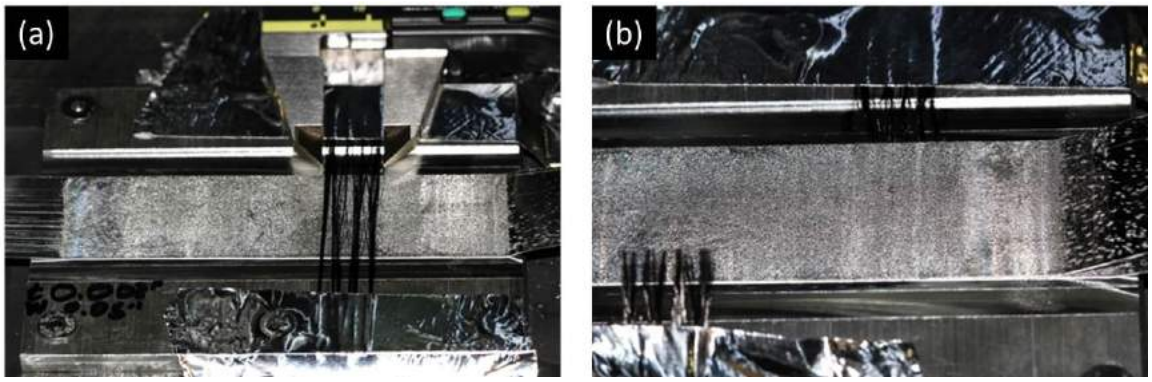

Figure 2.4: Embedding of a single CF bundle spread out and oriented perpendicular to tape feed. (a) Before embedding. (b) After welding one layer of tape over fibers.

2.1.2 UAM Parameters

For the first attempts at consolidating carbon fibers into aluminum, a set of optimal UAM process parameters were chosen that had been determined in a prior study [32]. The parameters used are shown in Table 2.1.

Table 2.1: UAM parameters used for single bundle embedding.

Welding Force	5000 N
Welding Speed	508 cm/min
Amplitude	32 μm
Heat-plate Temperature	Room Temperature (22 C°)
Spot Dwell	250 ms

2.1.3 Discussion

Macroscopically, it is apparent that none of these initial attempts to embed carbon fibers in aluminum would be suitable for use in integrated carbon fiber to metal joints

because of the damage at the aluminum tape edge. Within the aluminum structure, however, the consolidation quality of the carbon fibers was more promising. Scanning Electron Microscopy was used to evaluate the quality of the fiber consolidation. Pictured in Figure 2.5, the embedded fibers show little signs of damage with only a few cracked fibers. The aluminum flow around the fibers was excellent with no voids. These results suggest that embedding fibers in the manner described could be useful for applications such as material reinforcement. Material reinforcement is not the focus of this research project, though other projects within the SMSL may investigate CF as structural reinforcement in the future.

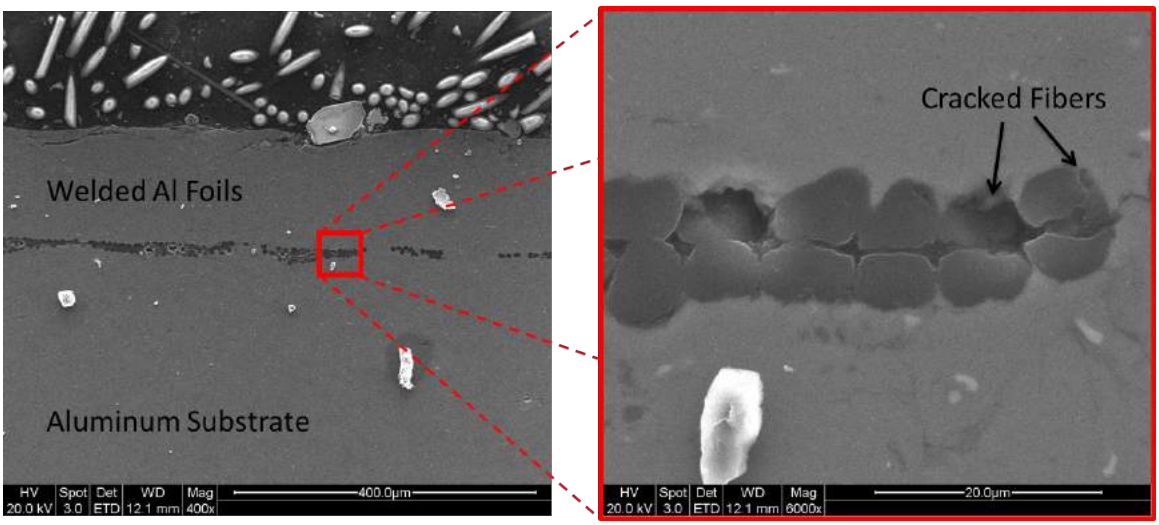

Figure 2.5: SEM images of embedded spread out carbon fiber bundle.

2.2 Embedding of Single CF Bundles With Channels

2.2.1 Joint Preparation and Results

As described in the previous section, the initial attempts at embedding carbon fibers were somewhat successful, but did not preserve the continuity of the fibers at the welded tape edge. To solve this problem, channels were cut in the aluminum substrate to house the carbon fiber bundles. The channels were cut with a 3.175 mm straight end mill after several layers aluminum tape had been welded over the aluminum substrate. Different channel depths were tried to empirically determine a depth that would prevent damage to the CF yet provide desired consolidation. For the channels of width 3.175 mm, a depth of 0.15 mm was found to prevent the CF bundles from shearing at the tape edge upon embedding. In Figure 2.6(b), notice that foil was torn on over the left most embedded CF. This occurred because the channel depth in that location was only 0.10 mm. Variation in channel depths was an issue that arose because of the non-level surface produced by the UAM process.

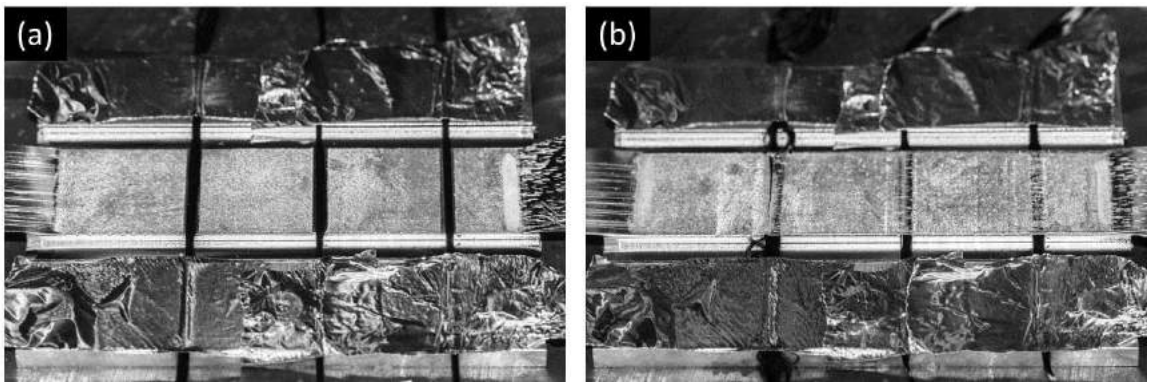

Figure 2.6: Embedding single CF bundles with channels to house the fiber bundles. (a) Bundles laid into channels prior to embedding. (b) Embedded CF bundles.

2.2.2 UAM Process Parameters

The weld parameters used were the same as those used for the initial embedding attempts, shown in Table 2.1.

2.2.3 Discussion

SEM images of the CF bundles embedded with aid of channels show very little damage done to the fibers. The amount of aluminum penetration was limited to the outer periphery fibers. This penetration would be improved by increasing the sonotrode oscillation amplitude during embedding. Greater aluminum penetration is desirable as it increases the mechanical interlocking between the CF and aluminum which, in turn, increases joint strength. It must also be considered, however, that raising the sonotrode amplitude increases chances of harming the fragile embedded fibers. Further research may be focused on finding the optimum welding amplitude to maximize aluminum flow while maintaining the structural integrity of the embedded fibers.

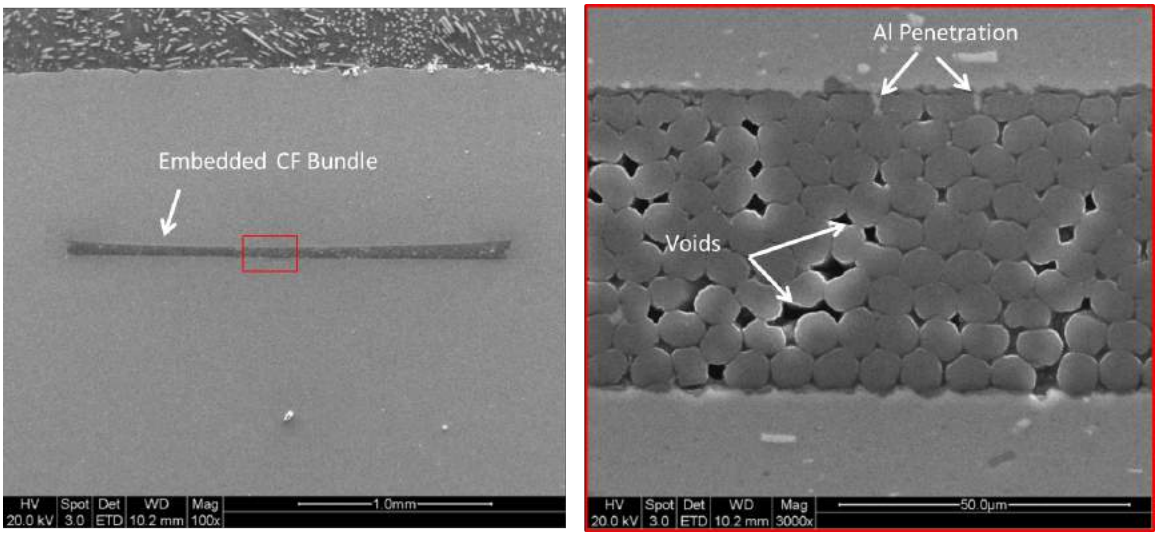

Figure 2.7: SEM images of embedded CF bundle in channel.

2.3 Mechanical Testing

The goal of encapsulating carbon fibers in this research is to create robust integrated CF to aluminum joints. In order for the joining method to be superior to the current industry standard, the joint strength needs to be comparable or greater than adhesive lap joining. For initial joint strength evaluation, pullout testing was chosen to determine the interfacial joint strength of single embedded carbon fiber bundles.

2.3.1 Testing Design and Setup

For the test, single CF bundles were embedded with the aid of relief channels as described in Section 2.2. Test specimens were machined out of the welded build, shown in Figure 2.8. During testing, the largest stresses occur within two bundle diameters from the front edge of the joint [18]. To be safe, the length of the CF to aluminum joint interface was set to five times of the effective CF bundle diameter (2.54 mm). Wood veneers were added to the free end of the carbon fiber bundles to avoid crushing from the tensile loading grips.

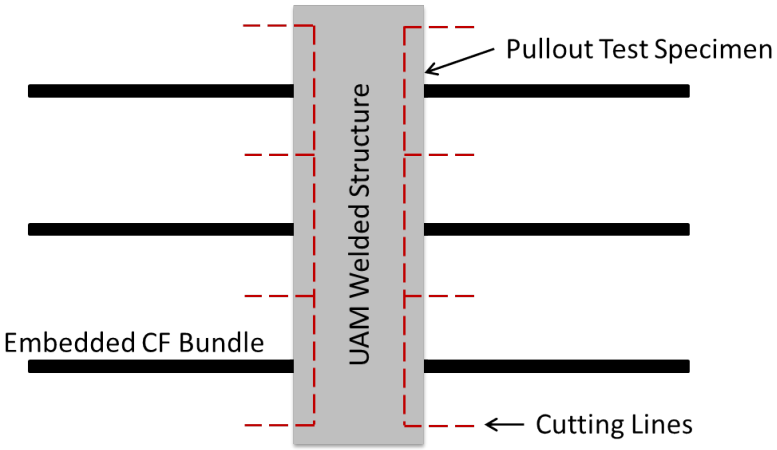

Figure 2.8: Schematic showing pullout test specimen construction.

A small load frame equipped with wedge type mechanical grips and load accuracy of 1.3 N was used to perform the pullout test. To hold the welded joint end of the specimen, a custom test fixture was used. This fixture had been used previously for interfacial strength testing of embedded NiTi fibers [14].

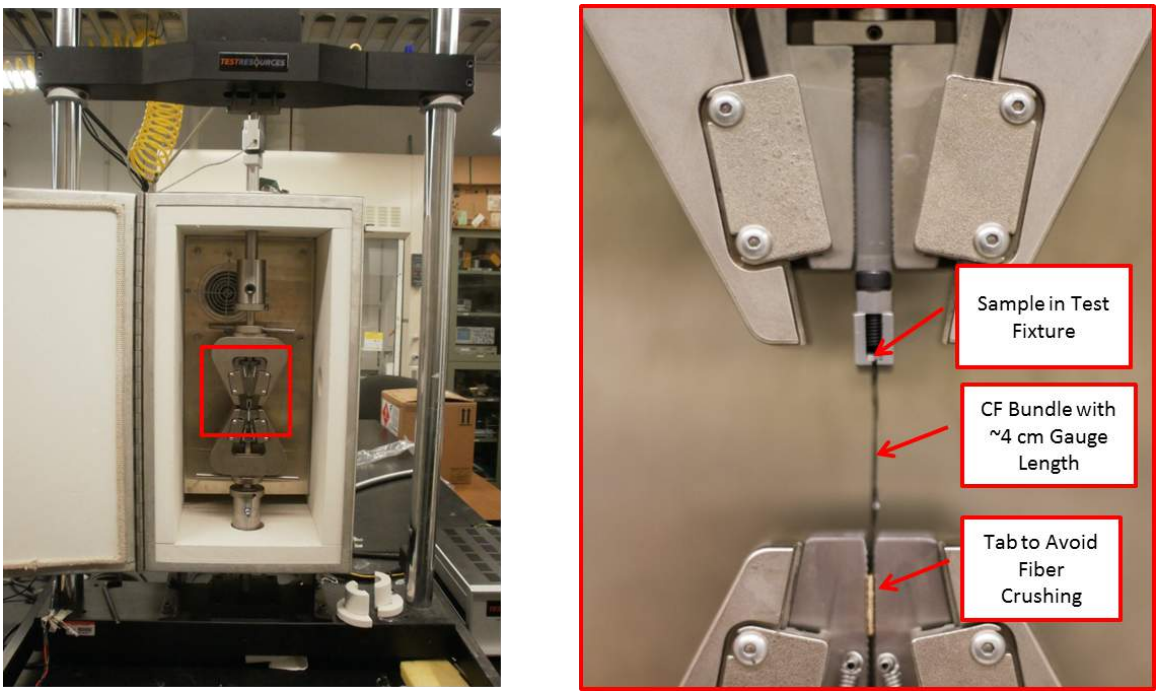

Figure 2.9: In house load frame with pullout fixture for embedded fiber pullout strength test.

2.3.2 Dry Carbon Fiber Pullout Results

The results from the pullout test with dry fibers showed that the joint strength was weak with the strongest joint only withstanding 20 N before pullout occurred. The fiber bundles did not pull out cleanly. The fibers around the edges of the bundles broke off while the interior fibers pulled out of the joint completely. This implies that periphery fibers were carrying the bulk of the loading because the interior fibers were not coupled with those at the joint interface.

Figure 2.10 shows the pullout specimens before and after testing to failure. The plot in Figure 2.12 shows the results from the dry pullout strength test compared with the joints in Section 2.3.3.

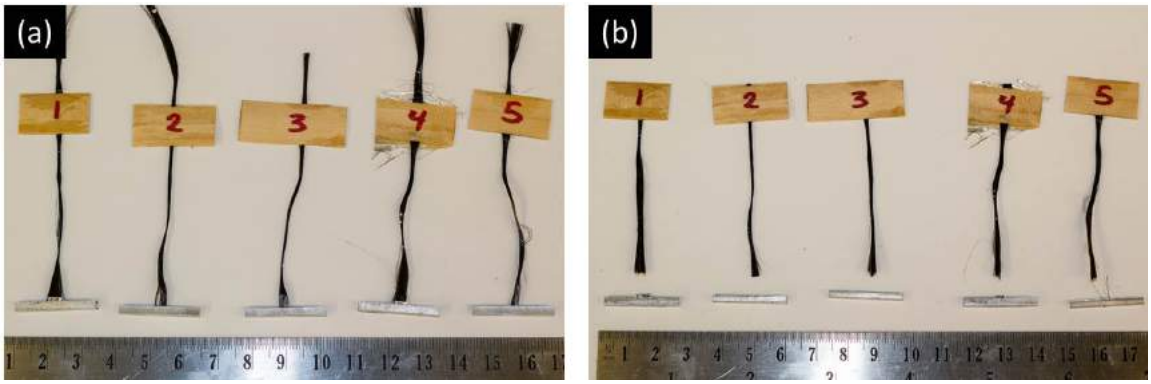

Figure 2.10: (a) Pullout strength test specimens before testing. (b) Specimens after failure.

2.3.3 Epoxy Wetted Carbon Fiber Pullout Results

In applications for carbon fiber to metal joints, dry fibers are formed into a composite using resin transfer molding techniques. Epoxy is used in this process to join the fibers together and effectively distribute the loading. It was therefore acceptable to complete the same pullout strength testing with the fibers having been wetted with epoxy. As pictured in Figure 2.7, the embedded carbon fibers feature small voids between fibers which allowed for epoxy to wick deep into the joint due to surface tension effects. The epoxy infiltrated through the joint allowed for more equal load distribution between the fibers. The result was that the joint strength increased by an order of magnitude from the dry fiber joint strength.

The fibers tested with epoxy performed superior to those without epoxy across the board. However, the the test samples with epoxy did not all fail in the same manner as seen in Figure 2.11. The joint on specimen E4 did not fail at all. Instead, the test specimen failed in the center of the gauge length. This test sample demonstrated that under the correct parameters an embedded carbon fiber joint can be stronger

than the carbon fiber itself. Figure 2.12 shows the results of the five test samples with epoxy.

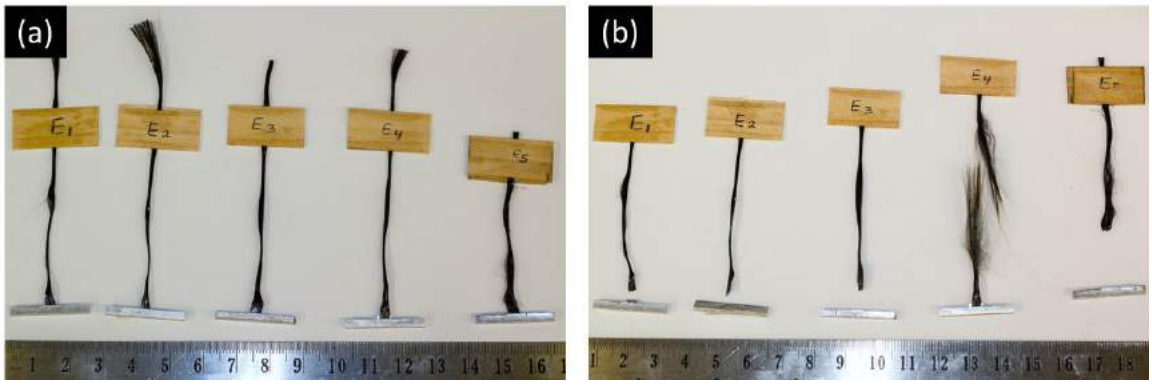

Figure 2.11: (a) Pullout strength test specimens with epoxy before testing. (b) Specimens after failure (right).

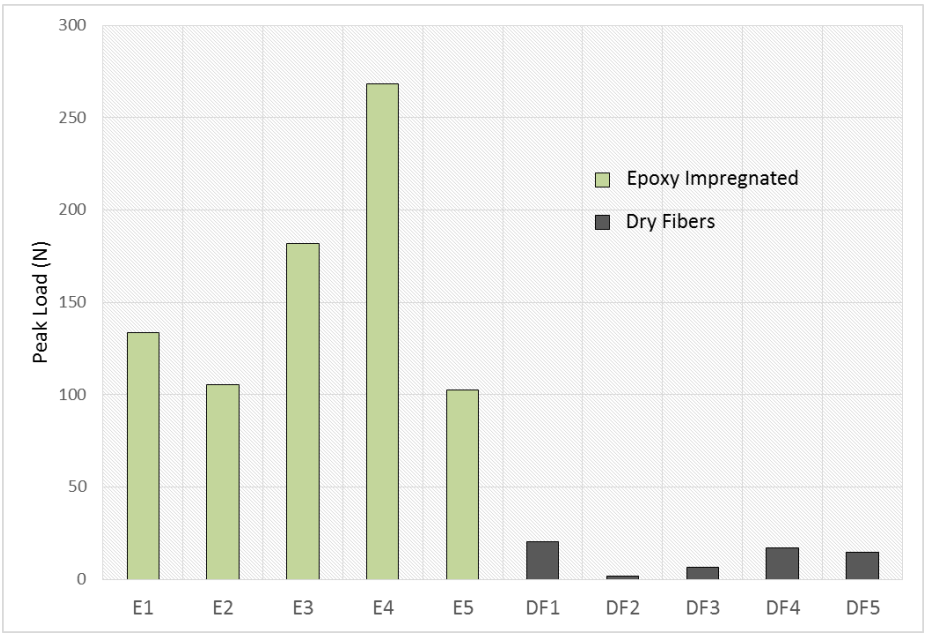

Figure 2.12: Pullout strength of epoxy impregnated joints compared with the strength of dry joints.

2.3.4 Analysis and Discussion

The results of the pullout strength testing suggests that the UAM process can be used to create joints that exceed the strength of carbon fiber. The pullout strength results also demonstrated the importance of wetting the joints with epoxy for maximized strength. Furthermore, the results showed that test specimens created using the same UAM parameters and same construction geometries yielded very different levels of strength. The variance in joint stength comes from the different failure modes present. The failure modes observed in the epoxy wetted test specimens include the following:

1. Clean pullout of bundle - Figure 2.13(a)

2. No joint failure, failure within the CF bundle - Figure 2.13(b)

3. Brittle fracture near the front edge of the joint - Figure 2.13(c)

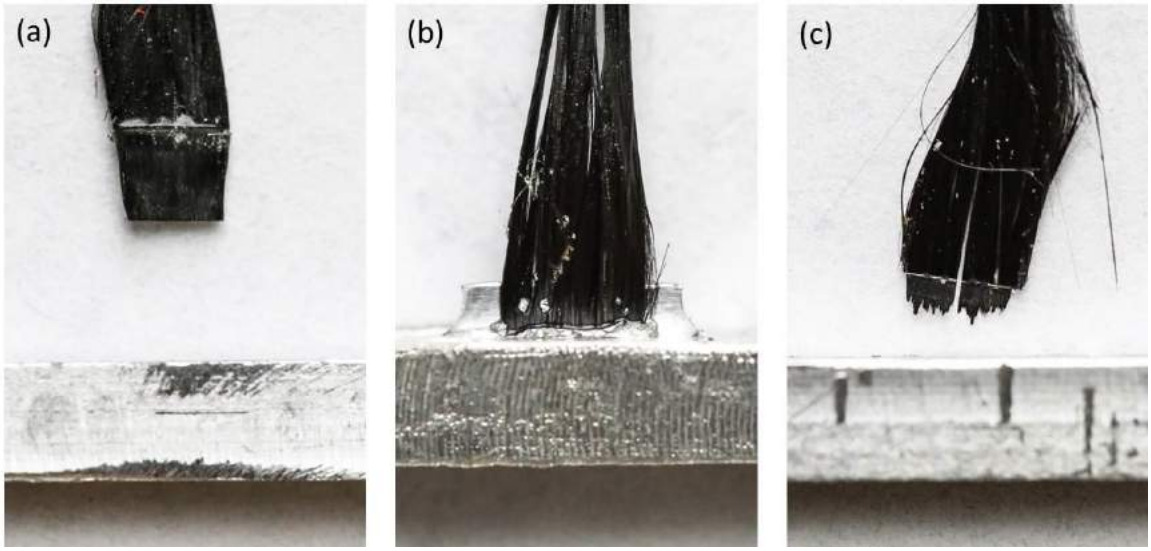

Figure 2.13: Three different failure modes seen in CF - Al joints wetted with epoxy. (a) Specimen E3, complete pullout from joint; (b) Specimen E4, failure in the fiber gauge length - no joint failure; (c) Specimen E5, brittle failure near the front edge of joint.

The different failure modes observed indicate variability in joint construction. Identical welding parameters were used to construct the test specimens, however, welding parameters including force and oscillation amplitude fluctuate significantly during the welding process. This is discussed further in Section 3.1.

Another reason for the different levels of joint strength is variability in channel depth used while embedding the fibers. The first failure case with clean pullout of the bundle occurred because of a lack of mechanical interlocking between the CF and aluminum. This lack of aluminum flow amongst the CF is due to the channel being too deep. The second case where the joint did not fail during testing represents

the desired joint characteristics. In the final failure case listed above, brittle fracture near the front edge of the joint was probably due to a slight crushing of the fibers during the welding process. Crushing generally occurs when the channel depth is not deep enough. In summary, to develop consistent joint strength, the proper channel size must be determined and maintained. The CNC mill has extreme accuracy to control the level of the bottom of the channels. However, the weld surface is not necessarily flat because fluctuations in the UAM welding parameters. Better methods for maintaining an even welding surface may be necessary for future joint optimization development.

2.4 Embedding of Half Density CF Bidirectional Textile

Applications for aluminum to CF joints involve CF parts made with bidirectionally woven textiles. This is the end goal of desired embedding capability. However, due to the high fiber density and complex channel geometry needed for embedding bidirectional CF textiles, initially half of the fibers in bidirectional CF textiles were removed. Embedding of half density bidirectional textiles was a stepping stone leading towards embedding the full density of fibers.

2.4.1 Joint Design and Preparation

The CF textile used for embedding was a mid-grade CF product designed for hobbyist aircraft construction. The fabric bundle spacing was 4.72 bundles/cm (12 bundles/inch). The joint was designed for each channel to house two CF bundles. This resulted in a channel spacing of 4.24 mm. The width of the channels were 1.99 mm. This narrower channel width was chosen to provide maximal weld substrate surface area. Similar to the earlier builds, a detachable 6061 aluminum base was used as

the initial substrate. A thickness of approximately 0.53 mm of aluminum tape was welded on the base-plate prior to the milling of the channels.

2.4.2 UAM Process Parameters

The UAM process parameters used for embedding the half density bidirectional CF textile were the same as those listed in Table 2.1.

2.4.3 Results

Initially, a nominal channel depth of 0.25 mm was chosen. However, severe tape tearing occurred with this channel depth. Further attempts with deeper channels proved to provide better bonding and eliminate tape tearing in the first layer over the fibers, seen in Figure 2.14(d). However, after several successive layers, slight tearing was seen. This was probably due to poor UAM control stability while welding over the irregular surface following CF embedding.

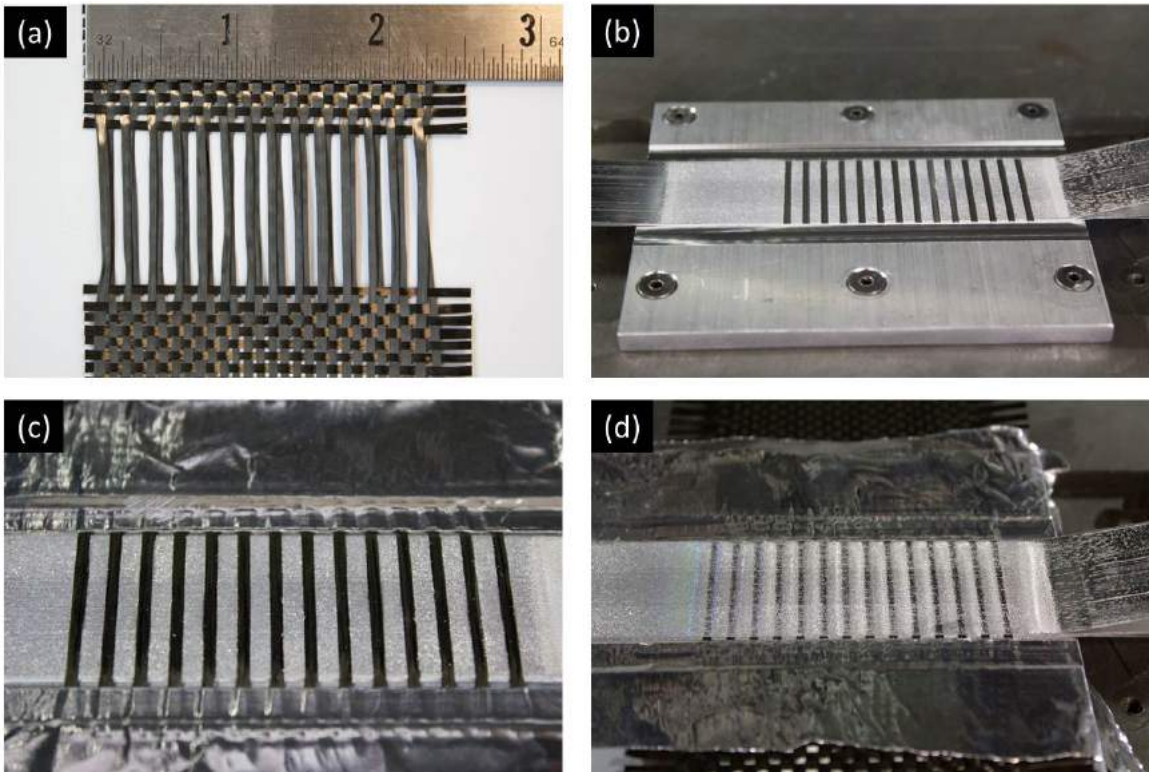

Figure 2.14: (a) CF textile preparation with horizontal fibers removed in the weld region. (b) Channels cut to house the CF bundles. (c) CF bundles secured in place prior to welding. (d) First layer of aluminum tape welded over CF textile.

2.4.4 Joint Integrated into CF Structure

Further foil layers were welded over the CF until the voids in the channels were reduced and torn tape layers were covered. At this point the CF to aluminum joint was removed from the base-plate and integrated into a CF structure. The steps of this process are shown in Figure 2.15.

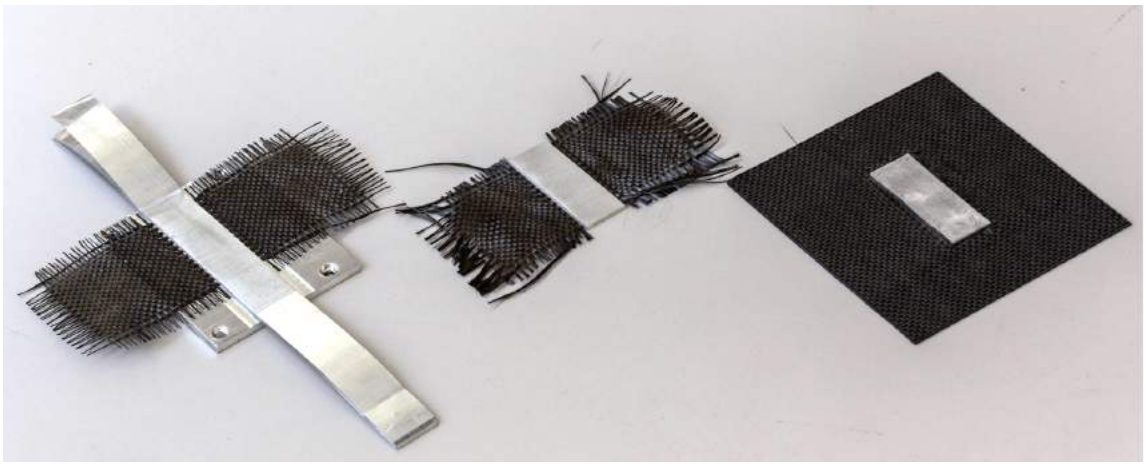

Figure 2.15: Progression of removing CF to aluminum joint from baseplate and integrating into CF structure.

2.5 Embedding of Full Density CF Bidirectional Textile

In actual application, CF to aluminum joints would be used as metal attachment points so that CFRP parts may be easily joined to surrounding metal structures. During the process of welding the attachment point material over a CF textile, the importance of preserving the full CF density should not be understated. There are two main reasons for this:

1. Preserving the full density of embedded CF results in more load supporting fibers which leads to stronger joints.

2. Removing fibers requires precise cutting and removal of unwanted fiber bundles. This would require an additional tedious manufacturing process if adapted by industry.

2.5.1 Joint Design and Preparation

Embedding full density bidirectional CF fabric presents several new difficulties over embedding unidirectional fabric. First and foremost, the physical area of the aluminum surface being welded over is reduced to pillars due to the bidirectionality of the channels used to house the CF. This reduced substrate area requires a lower than optimum welding force to avoid excessive plastic deformation of the pillars surrounding the CF. The smaller weld area also reduces the joint strength between layers of welded tape. This inter-layer joint strength is directly proportional to the weld area. The smaller area also increases the compliance of the weld region which can lead to poor inter-laminate bonding.

Secondly, the geometry of the CF used requires channel width be increased to from 1.59mm to 2.29mm. This greater channel width increases possibilities for tape tearing. Issues with torn tape proved to be the greatest hurdle for embedding full density bi-directional CF fabric.

Because of the woven nature of bidirectional CF, the channel depth was increased at the channel intersection points, shown in Figure 2.16. The nominal depth of the channels was 0.33mm and the depth at the intersection points were cut out to a depth of 0.38mm. The spacing of the channels remained at 4.23mm since the CF used was the same material described in Section 2.4.1.

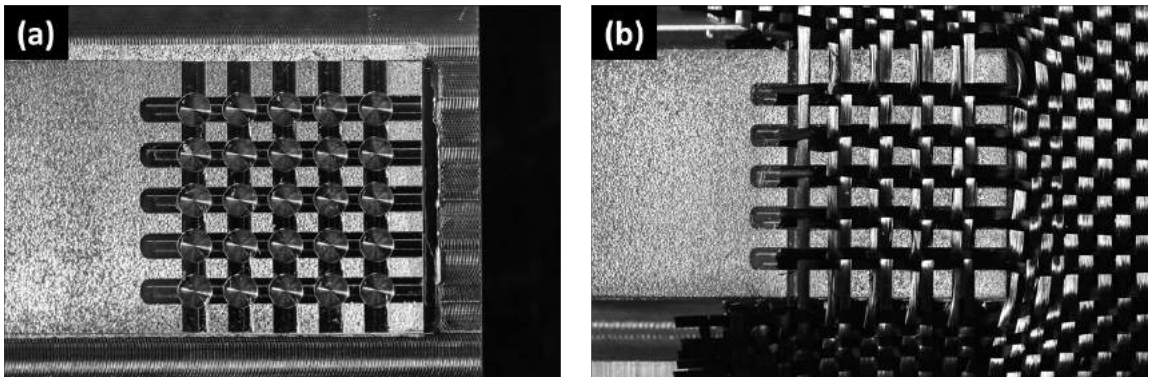

Figure 2.16: (a) Channels geometry used to embed bidirectional CF. (b) Fibers placed into channels prior to embedding.

2.5.2 UAM Process Parameters

The initial UAM parameters used for embedding the the bidirectional CF textile are listed in Table 2.2. These parameters were used to successfully embed the fibers, however, there was substantial tape tearing present. A number of other UAM parameter combinations were tried with little success in reducing the amount of tape tearing. It was discovered that one of the main causes of the tape tearing issue was the UAM controller instability. After the controller was modified, a new set of parameters shown in Table 2.3 were used which resulted in no tape tearing. The issue of controller instability is discussed in Chapter 3.

Table 2.2: Initial UAM parameters used embedding bidirectonal CF textile.

Welding Force	3000 N
Welding Speed	254 cm/min
Amplitude	31 μm
Heat-plate Temperature	Room Temperature (22 C°)
Spot Dwell	250 ms

Table 2.3: Final UAM parameters used embedding bidirectional CF textile.

Welding Force	3000 N
Welding Speed	508 cm/min
Amplitude	31.5 μm
Heat-plate Temperature	Room Temperature (22 C°)
Spot Dwell	250 ms

2.5.3 Results

As previously mentioned, embedding bidirectional CF fabric requires a much smaller weld area. This requires the UAM process to work in a range that is near its limit for creating joints with high structural integrity. The initial attempts of embedding the bidirectional CF fabric resulted in moderate success. None of the fibers were damaged or crushed. However, tape tearing continued to be an issue as seen in Figure 2.17. Further developments including the downforce stability study discussed in Section 3.1 were performed in an effort to eliminate tape tearing. The outcome of the downforce study was altered controller gain. The controller modifications smoothed out the variation in the weld force enough to eliminate any tape tearing (Figure 2.18) when using the parameters shown in Table 2.3.

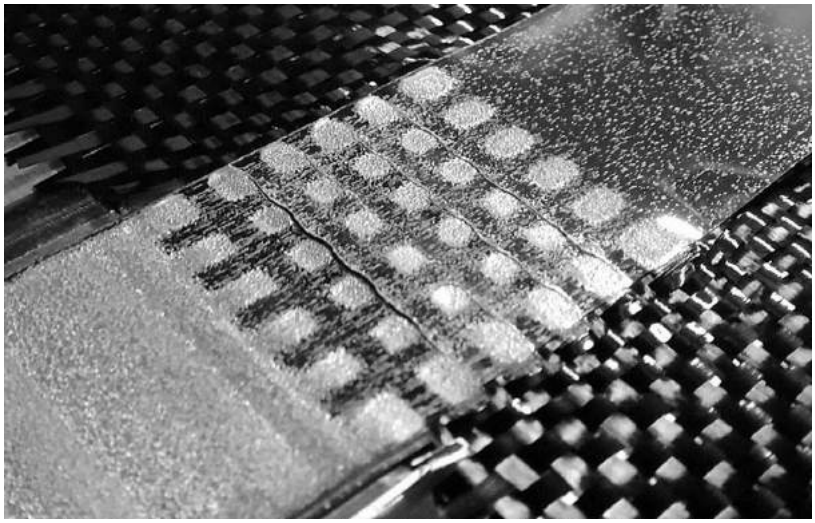

Figure 2.17: Tape tearing after first embedding layer.

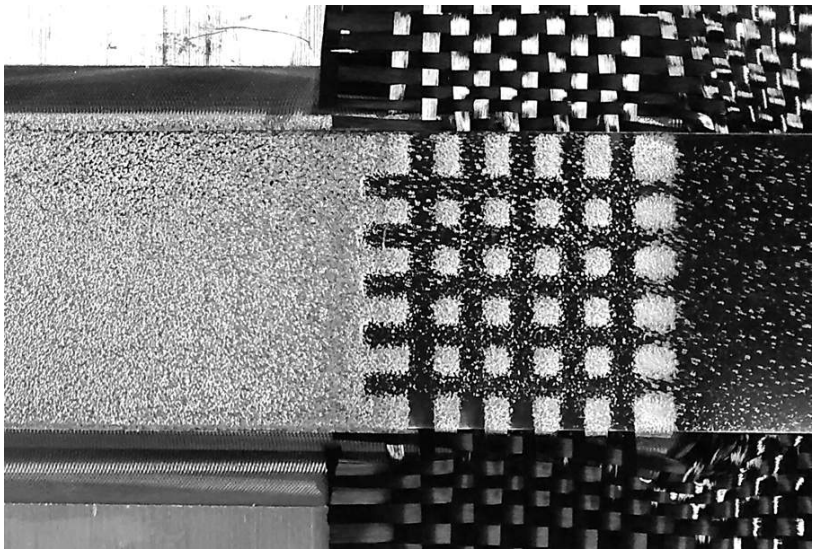

Figure 2.18: First aluminum tape layer welded over bidirectional CF textile with no tape tearing.

Upon further investigation of the embedded bidirectional fabric by optical microscopy, it was found that the consolidation quality varied greatly depending on orientation of the embedded CF. Fibers embedded perpendicular to the weld direction exhibit clear lines between the aluminum laminate layers. This indicates poor bonding as seen in Figure 2.19(a). Comparing Figure 2.19(a) with (c), the CF bundle from (a) is much thinner and more spread out. Fibers bundles embedded parallel to the weld direction, (c), were not as wide because the aluminum pillars on either side of the channel deformed, flowing into the channel and packing the fibers in the middle. This resulted in a much cleaner looking joint, indicating good bond strength.

The closeup images from parallel and perpendicular orientations in Figure 2.19(b) and (d) both show desirable aluminum penetration into the carbon fibers. The penetration is not limited to the periphery fibers. Rather, aluminum can be seen all the way in the middle of the embedded bundles. A possible reason for the increased aluminum penetration from what was seen earlier in Figure 2.7 is the addition of using alcohol in the joint preparation procedure. Wetting the fibers while positioning them into the channels causes the fibers to densify upon evaporation of the alcohol. While on the topic of the closeup images, it should be noted that the black areas between fibers are merely positions where the fibers were cut short during the sample preparation. They appear as deep voids only because of the shallow depth of field of the optical microscope.

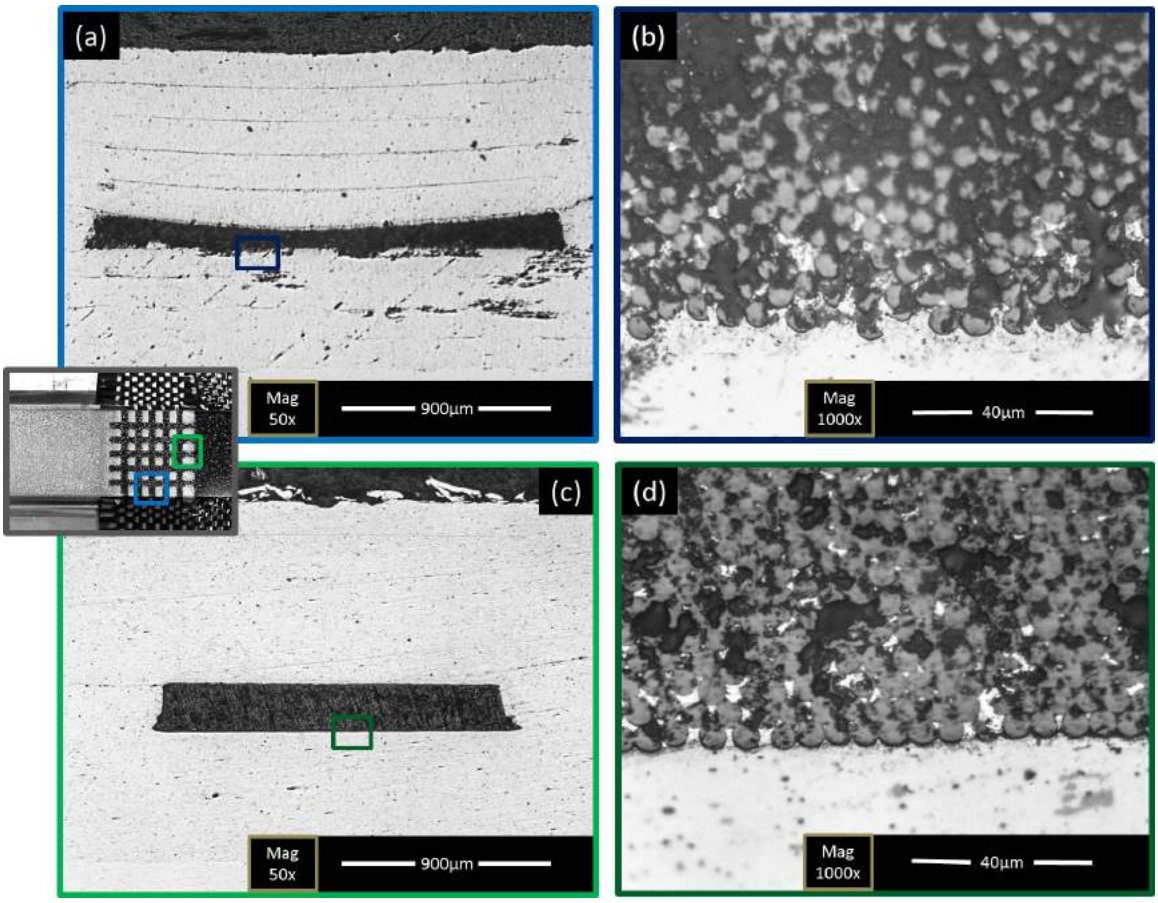

Figure 2.19: Comparison of embedded CF from different locations of the joint. The light gray speckles between the carbon fibers in the closeup images is penetrated aluminum. (a) Embedded CF perpendicular to weld direction. (b) Closeup of (a). (c) Embedded CF parallel to weld direction. (d) Closeup of (c).

CHAPTER 3

MANUFACTURING CONTROL

3.1 Downforce Stability

As previously mentioned in Section 2.5.3, intermittent tape tearing occurred when embedding the bidirectional CF textile. The severity and location of the tearing was not predictable, even when given identical welding parameters and identical build geometry. It was hypothesized that poor downforce control was the cause of the inconsistent tape tearing. To investigate the weld downforce profile, the UAM diagnostics were setup to record the force measured by the machine's load cell during the welding operation. For further analysis, the data was retrieved from the machine and filtered to smooth out the uneven traces due to the 50 Hz sampling rate.

3.1.1 Force Profile Before and After Controller Modification

After reading in the force profile for the first time, it was apparent that there were load control stability issues. As seen in Figure 3.1, the profile before the gain was decreased exhibited oscillating swings of about 1000 N about the nominal force value of 3000 N. The frequency of the oscillations was about 4 Hz. The cause of the oscillating behavior is not completely understood. The load cell natural frequency is 10 Hz.

This rules out the possibility of a resonant mode being excited in the load cell. It was supposed that the the controller settings may have excited a resonant frequency in the UAM center table. In any case, as seen in Figure 3.1, by lowering the gain of the controller, the downforce profile was smoothed out considerably.

The UAM controller does not use true PID control, though the control algorithm is very similar to PID with C_1x, C_2x^2, and C_3x^3 terms. The term that was modified was the controller gain. It was reduced from $5x10^{-5}$ to $5x10^{-7}$. Several other parameters were also adjusted that were associated with the bounds corresponding to different response speeds. These bound parameters have little to no effect on the downforce profile while embedding fibers because the bounds only come into affect when the measured force is within +/-2% of the nominal force value.

The region affected by the downforce instability was the embedding area over the fibers. Due to the added compliance over in the embedding region, the weld force was reduced initially until the weld head displacement was able to catch up with the irregular surface. It was originally hypothesized that sudden increases in the down force were a direct causes of tape tearing. However, after comparing force plots with actual build tape tearing, no distinct correlations between changes in force and tape tearing could be found.

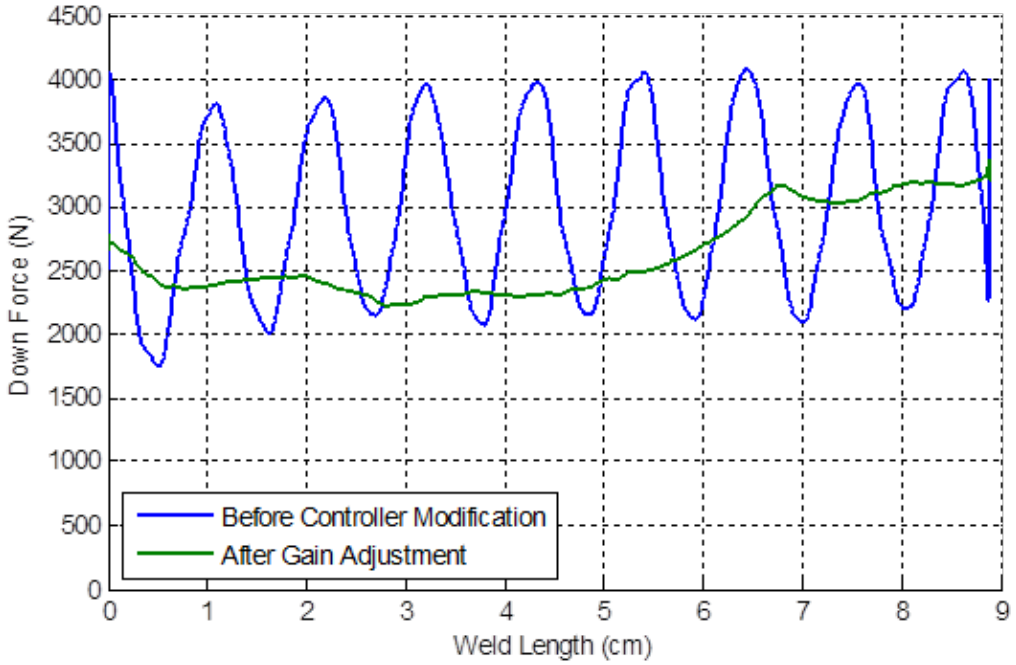

Figure 3.1: Downforce profile during the length of a even weld before and after controller gain adjustments.

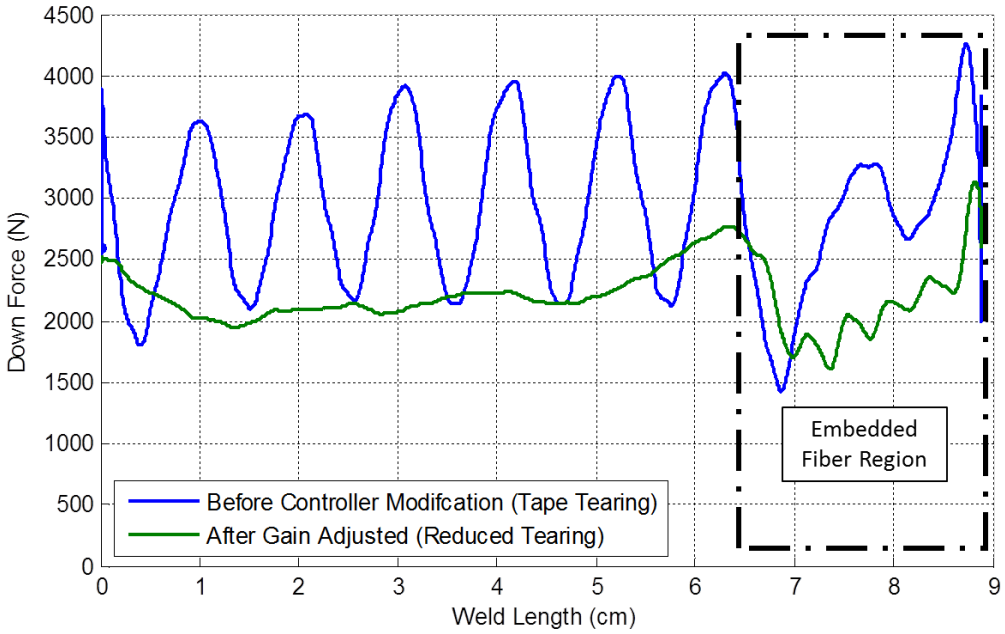

Figure 3.2: Downforce profile during the first layer of foil embedding bidirectional CF fabric before and after controller gain adjustments.

Even though there is not hard evidence that sudden changes in welding force causes tape tearing, there is evidence that welding with the modified controller gain produced better results when embedding the carbon fibers. With the reduced gain, tape tearing was still present, but was less severe. To better quantify the stability of the downforce when embedding the bidirectional fabric, average standard deviations for the downforce and weld power over each channel were calculated. It was found that the variation in the weld force was reduced by a factor of two with the lower controller gain. Conversely, the average of the standard deviation of the welding power over the channels did not change greatly after the lower controller gain was implemented. The standard deviation results are depicted in Figure 3.3.

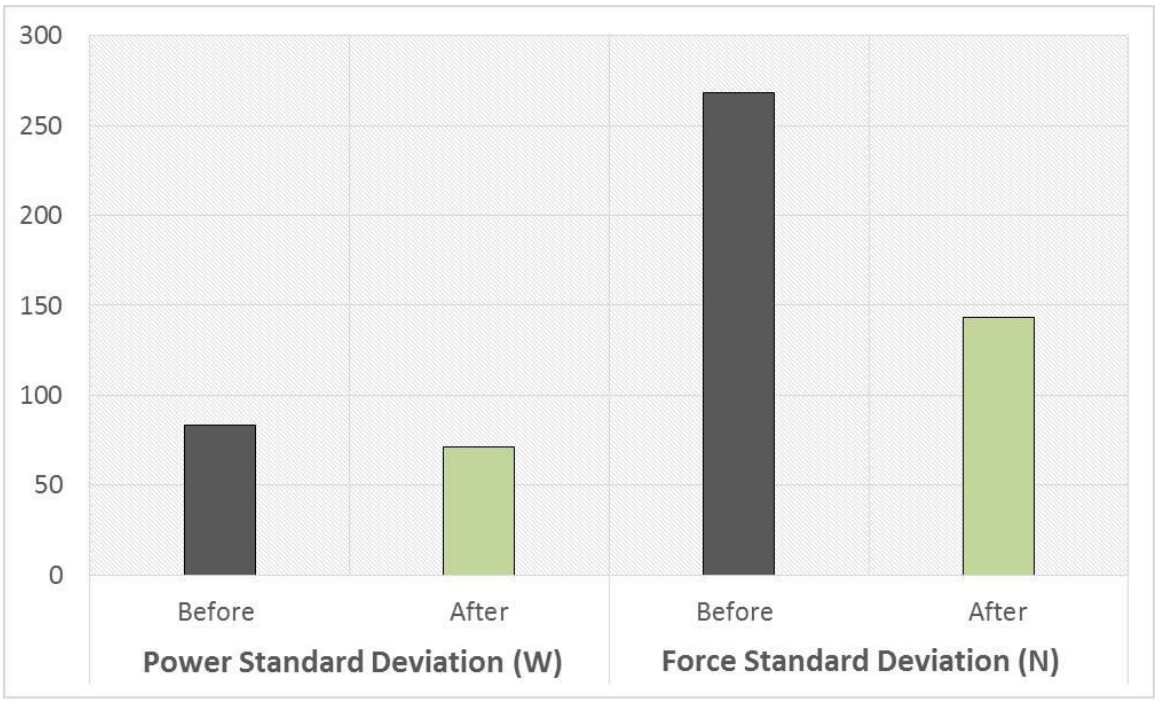

Figure 3.3: The average of standard deviation over individual channels during the first layer of welded foil over the channels.

3.1.2 Effect of Welding Speed

Even after reducing the gain in the controller by a factor of 100, most of the welds embedding the bidirectional CF fabric still exhibited tape tearing. The welding speed used prior to embedding the bidirectional fabric was 508 cm/min. For the bidirectional fabric, the weld speed had been slowed to 254 cm/min in an effort to help the controller respond to the uneven surface. However, it was found that by increasing the weld speed back to 508 cm/min, tape tearing was completely eliminated. There are two likely causes for this:

1. The doubled weld speed effectively slows the controller downforce response with respect to displacement by a factor of two. Though the controller gain does not

change, the weld head sees the uneven substrate geometry twice as fast. This essentially allows the welding to occur before the controller can command a harsh movement that would cause the tape tearing.

2. The doubled weld speed means that the overall energy going into the weld cut in half. The smaller amount of energy could allow the welding to occur without severing the tape over the channels.

The first point made is the reason for the lower force in the embedding region for the faster weld speed shown in Figure 3.4. The lower force also causes a slightly lower power throughout the embedding region which further reduces the energy going into the weld. The second point made, while making a case for why tape tearing is eliminated, also indicates that the amount of aluminum flowing into the carbon fibers will is reduced. This suggests that the amount of energy going into the weld is a tradeoff between avoiding tape tearing and still maximizing weld quality and aluminum penetration.

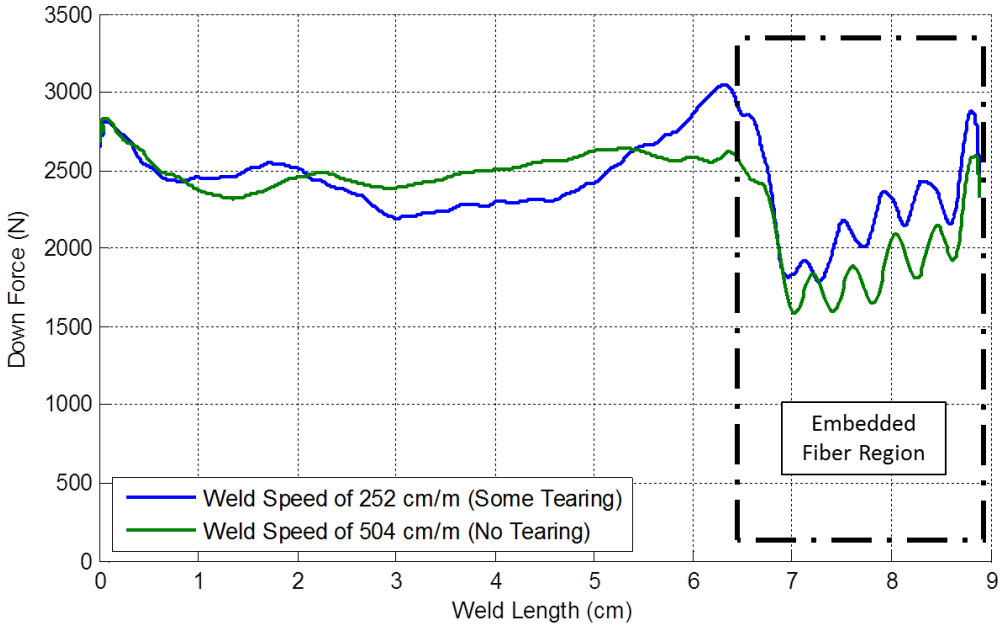

Figure 3.4: Effect of weld speed on force profile while welding first layer of aluminum tape over bidirectional CF fabric.

3.1.3 Discussion

The results from the downforce stability study show that lowering the controller gain was an improvement to the UAM system. The modified force response no longer overshot the nominal force value, remaining much smoother and constant. The lowered controller gain combined with proper welding parameters (including weld speed) enabled embedding of bidirectional CF fabric without tape tearing. It should also be noted that the channel depth has a huge influence on whether tape tearing occurs. This is not completely understood, because in every case, the height of the CF was less than the depth of the channels. To eliminate the tearing, it was necessary to make the channels twice as deep as the height of the CF. This resulted in a welding surface with very uneven compliance in the embedding region.

3.2 Substrate Compliance Model

The force profiles in the embedding regions of Figures 3.2 and 3.4 suggest the compliance of the substrate during welding has a large influence on the welding force and welding power. The compliance of the structure over the embedding region has a prominent impact on inter-laminate bonding quality. Due to the channel geometry and radius of the sonotrode, the actual down force experienced by the aluminum tape over the center of the channels was much less than Figures 3.2 and 3.4 show. This is because due to the greater depth of the channel and lessor depth of carbon fibers in the channel, the bulk of the weld force is distributed along the channel walls. The result is very poor inter-laminate bonding above the channels. This is easily seen the cross section image in Figure 3.5.

For the reasons discussed, a compliance model comparing the build effective stiffness throughout the weld length is beneficial toward progressing to further joint designs. For simplicity, only several key positions on along the weld length were considered.

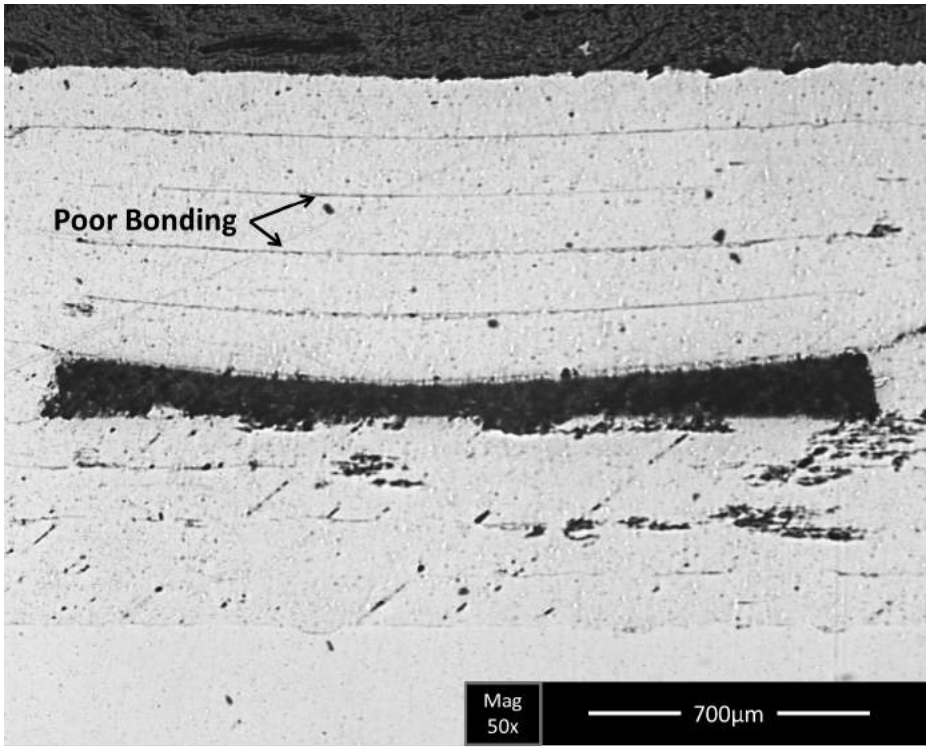

Figure 3.5: Cross section of embedded bidirectional CF fabric with very poor inter-laminate bonding over the embedded fibers.

3.2.1 Material Properties and Joint Geometry

The joint geometry used for this compliance analysis was based on the design and dimensions used to embed bidirectional CF fabric, described in Section 2.5. Material properties were assumed nominal values for the given substance. It should be noted that the elastic modulus of the carbon fiber may be different than the value used in the analysis. Carbon fiber is a not an isotropic material. The elastic modulus parallel to a theoretically perfect carbon fiber is 1,060 GPa while the modulus perpendicular to the same fiber is 36.5 GPa [16]. Practically speaking, however, carbon fibers are never aligned perfectly to their crystal structure. Therefore, the modulus parallel to

the fibers is typically far less than the maximum theoretical value and the modulus perpendicular to the fibers is much greater than the theoretical value. For this analysis an estimate of 100 GPa was used for the modulus perpendicular to the fibers. It should also be noted that the thickness defined for the CF, t_{CF}, is less than the depth of the channels, t_{ch}. This is accurate to the geometry which was used for embedding bidirectional CF fabric discussed in Section 2.5 and creates several loading cases that will be discussed in Section 3.2.2.

Table 3.1: Joint geometry constants and material properties used in compliance model.

Description	**Variable**	**Value**
Total width of weld	w_t	25.4 mm
Width of channels	w_{ch}	2.29 mm
Width of aluminum pillars	w_p	1.95 mm
Thickness of base layers	t_b	0.51 mm
Depth of channels	t_{ch}	0.33 mm
Height of CF	t_{CF}	0.20 mm
Thickness of aluminum tape	t_T	0.15 mm
Number of lengthwise channels in total width	n_{ch}	5
Sonotrode diameter	D_s	96.52 mm
Hertzian contact width at 3000N	w_{hc}	0.87 mm
Loading from sonotrode	F	3000 N
Elastic modulus of 6061 aluminum	E_{al}	69 GPa
Elastic modulus of CF (Perpendicular to fibers)	E_{CF}	100 GPa

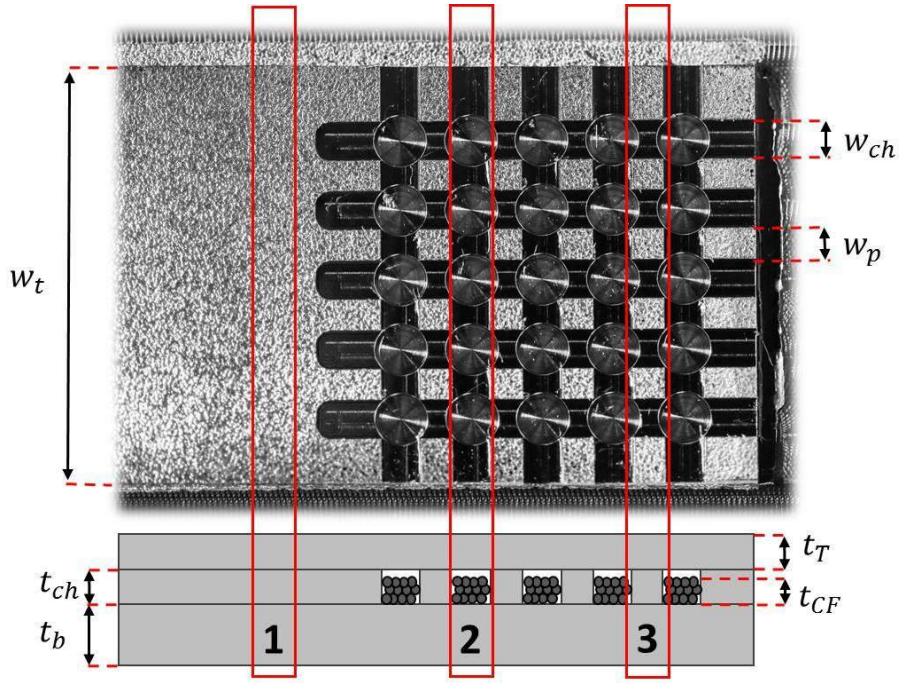

Figure 3.6: Schematic showing compliance model dimensions and annotating the three sections analyzed in Section 3.2.2.

3.2.2 Modeling Technique

To keep the compliance model as simple as possible and still gain important insight, three sections of the weld length were chosen for analysis, seen in Figure 3.6:

1. Region without any channels or embedded fibers. In this section the base layers and current layer of aluminum tape are lumped into a solid thickness of aluminum.

2. Region over channel with CF. The compliance in this section varies depending on loading assumptions. Three cases will be presented and discussed to account for the three possible loadings.

3. Region intersecting aluminum pillars between channels. Here the compliance also varies depending on if the fibers support load or not. These two cases will be discussed.

By comparing the compliance of these three sections a good estimate of overall compliance evenness is achieved.

In each region and for every case, the stiffness of the aluminum base plate is assumed to be infinite and therefore is not included in the modeling. In each case considered, the same width of hertzian contact, w_{hc} (defined in Table 3.1), is used. Each region stiffness is defined by assuming this width throughout the height of the build and assuming that there is no load sharing with the surrounding structure.

3.2.2.1 Region 1

Modeling the compliance of region 1 is very straightforward. The laminate layers of aluminum are treated as a solid structure. The result is a single stiffness component as seen in Figure 3.7. The stiffness of region 1 is shown in Equation (3.1), determined by the definition of stiffness of a bar [9].

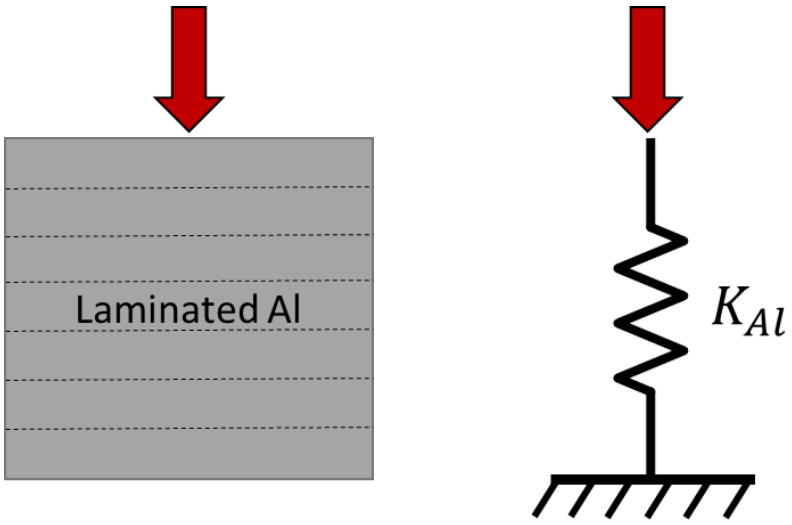

Figure 3.7: Region 1 of the compliance model.

$$K_{Al} = \frac{\mathrm{w_{hc} w_t E_{al}}}{\mathrm{t_{totalthickness}}} \tag{3.1}$$

3.2.2.2 Region 2

Region 2 is the most involved region of the compliance model. There are three possible cases considered, illustrated in Figure 3.8.

Case A assumptions:

- Loading acts only on the layer of aluminum tape bridging the channel.
- Stiffness of aluminum tape is modeled as a beam with fixed and roller end conditions.

Case B assumptions:

- Loading from sonotrode is exerted on the channel walls (pillars) after the tape has deformed in the center of the channel.

- Hertzian contact remains the same value, w_{hc}, as in the other cases.

Case C assumptions:

- Load is supported by the CF in the channel. (This occurs after plastic deformation in the channel walls, eliminating the mechanical mismatch between the height of the CF and the depth of the channel.)

- The carbon fiber is treated as a solid material with no air between fibers.

Expressions for the stiffness components from Figure 3.8 are shown in Equations (3.2) to (3.7). Equation (3.2) was found by using standard beam theory with fixed and roller end conditions [9]. The fixed end corresponds to the tape that has been welded. The roller end corresponds to the condition on the side of the channel not yet welded. Other stiffness components in Equations (3.4) to (3.7) were determined using the definition of the stiffness of a bar [9].

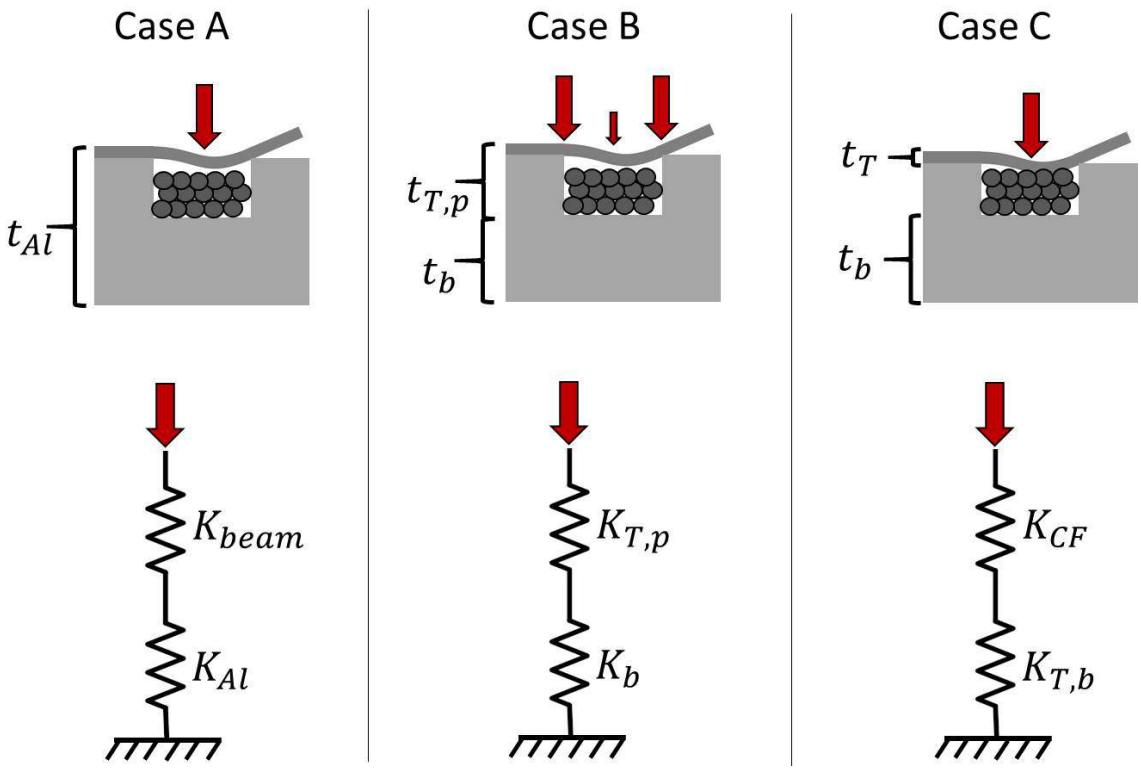

Figure 3.8: Region 2 of the compliance model.

$$K_{beam} = \frac{768\mathrm{E_{al}I}}{7\mathrm{w_{ch}^3}} \tag{3.2}$$

Where the area moment of inertia of the beam is shown in Equation (3.3) [9].

$$I = \frac{\mathrm{w_t t_T^3}}{12} \tag{3.3}$$

$$K_{T,p} = \frac{\mathrm{w_{hc}(w_t - 5w_{ch})E_{al}}}{\mathrm{t_T + t_p}} \tag{3.4}$$

$$K_b = \frac{\mathrm{w_{hc} w_t E_{al}}}{\mathrm{t_b}} \tag{3.5}$$

$$K_{CF2} = \frac{\mathrm{w_{hc} w_t E_{CF}}}{\mathrm{t_{CF}}} \tag{3.6}$$

$$K_{T,b} = \frac{\mathrm{w_{hc} w_t E_{Al}}}{\mathrm{t_T + t_b}} \tag{3.7}$$

The equivalent stiffness for cases A, B, and C are shown in Equations 3.8, 3.9 and 3.10 respectively.

$$K_{2A} = \left(\frac{1}{\mathrm{K_{beam}}} + \frac{1}{\mathrm{K_{Al}}} \right)^{-1} \tag{3.8}$$

$$K_{2B} = \left(\frac{1}{\mathrm{K_{T,p}}} + \frac{1}{\mathrm{K_b}} \right)^{-1} \tag{3.9}$$

$$K_{2C} = \left(\frac{1}{\mathrm{K_{CF2}}} + \frac{1}{\mathrm{K_{T,b}}} \right)^{-1} \tag{3.10}$$

3.2.2.3 Region 3

The third and final region under consideration includes the aluminum pillar area. There are two possible loading cases in this region, illustrated in Figure 3.9.

Case A assumptions:

- Load from the sonotrode is supported by the aluminum pillars, not the carbon fiber in the channels.
- Load is distributed evenly on the base layers throughout the width of the weld.

Case B assumptions:

- Loading from sonotrode is exerted evenly on the carbon fiber in the channels and the aluminum pillars.

- The carbon fiber is treated as a solid, with no air gaps between fibers.

Expressions for the stiffness components from Figure 3.9 are shown in Equations (3.7) to (3.12). Stiffness components were determined using the definition of stiffness of a bar [9].

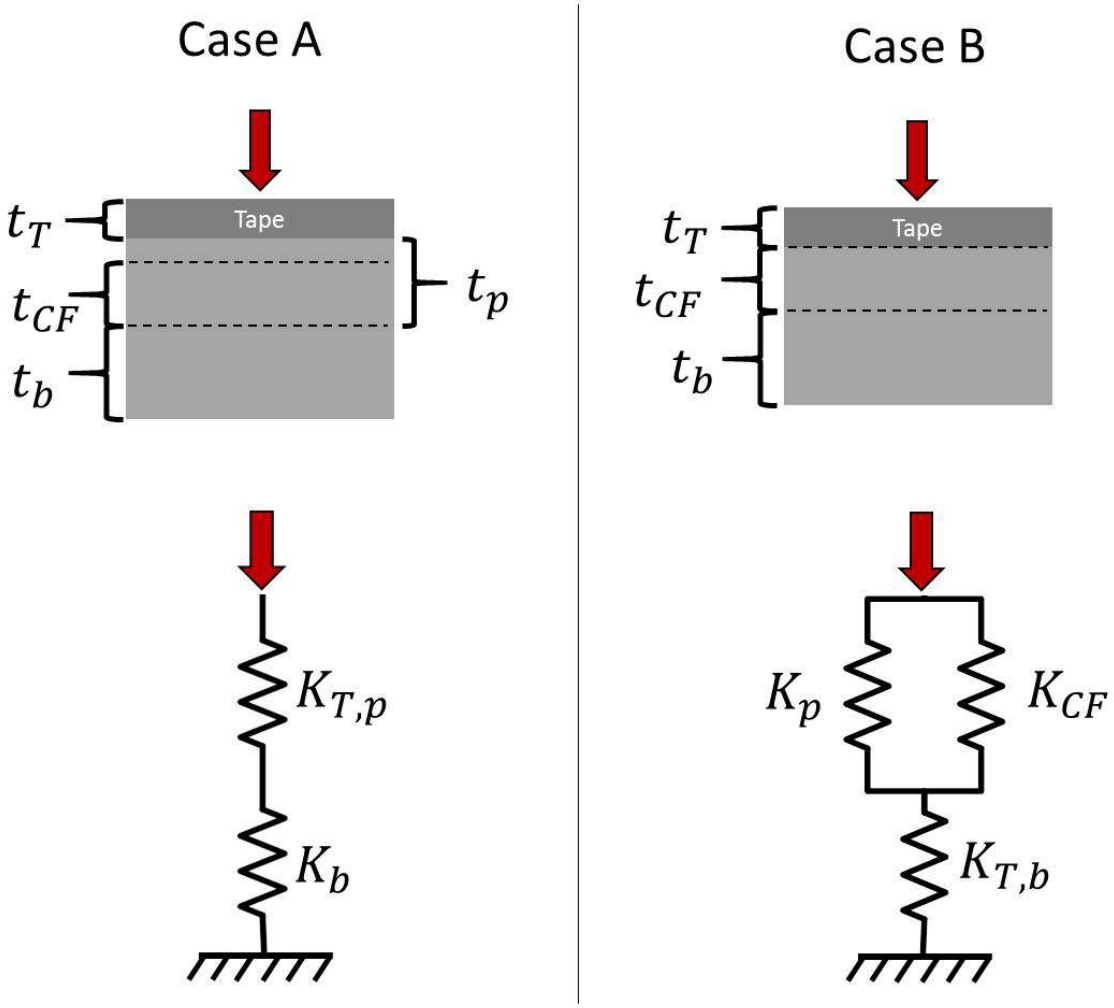

Figure 3.9: Region 3 of the compliance model.

$$K_p = \frac{\mathrm{w_{hc}(w_t - 5w_{ch})E_{al}}}{\mathrm{t_{CF}}} \tag{3.11}$$

$$K_{CF3} = \frac{\mathrm{5w_{hc}w_{ch}E_{CF}}}{\mathrm{t_{CF}}} \tag{3.12}$$

The equivalent stiffness for cases A and B are shown in Equations 3.13 and 3.14 respectively.

$$K_{3A} = \left(\frac{1}{\mathrm{K_{T,p}}} + \frac{1}{\mathrm{K_b}}\right)^{-1} \tag{3.13}$$

$$K_{3B} = \left(\frac{1}{\mathrm{K_p + K_{CF3}}} + \frac{1}{\mathrm{K_{T,b}}}\right)^{-1} \tag{3.14}$$

3.2.3 Results and Discussion

The results of the stiffness values for the compliance model are listed in Table 3.2. The only stiffness that differed greatly from the rest was Region 2, case A. This was the stiffness over the channel with the assumption that the CF did not carry any of the load. The low stiffness of this region results in high plastic deformation of the welded tape. This, while embedding the CF nicely, results in a highly uneven weld surface which in turn causes poor bonding over the channel regions.

Table 3.2: Compliance model stiffness values.

Region 1	**Region 2**			**Region 3**	
	Case A	Case B	Case C	Case A	Case B
1.54e9 N/m	4.46e6 N/m	1.21e9 N/m	1.91e9 N/m	1.21e9 N/m	1.77e9 N/m

It is apparent that the primary cause of uneven compliance during welding is due to Case A of Region 2. It would therefore seem acceptable to reduce the depth of the channels so that the channel depth matches the height of the carbon fibers. This would greatly reduce any changes in compliance throughout the weld length. Attempts were made to implement this change. However, anytime the channel depth was decreased, severe tape tearing occurred. To achieve even compliance throughout the weld length while maintaining zero tape tearing will require a slightly different weld design. This varied joint design is discussed further in Chapter 4.

CHAPTER 4

DESIGN FOR MULTI-PLY CF TO ALUMINUM TENSILE TEST SPECIMEN

The final objective of this project was to use knowledge gained from elementary CF to aluminum joints described in Chapter 2 along with understanding of weld force stability and subrstrate compliance from Chapter 3 to develop a design for a CF to aluminum tensile test specimen. This testing specimen would feature six layers of embedded bidirectional CF fabric. Following the welding process, the six layers would be formed into a composite structure with epoxy. The reason for six layers is because the grade of CF being used is about 0.254 mm thick per layer and the desired thickness of the carbon fiber composite is about 1.6 mm thick. This is the thickness specified by ASTM D3528 standard for double lap shear adhesive joints for tensile loading [1]. This standard is referenced because the aim is to test the 6 ply UAM CF to aluminum joint and compare its strength with adhesive double and single lap joints.

4.1 Initial Stacking Attempt

In order to create a tensile specimen build with six layers of embedded bidirectional fabric, the embedding method described in Section 2.5 must be used successively.

Adding layer upon layer of embedded CF requires that the weld quality is excellent. As further layers are embedded, increasingly uneven compliance in the z direction causes poor bonding over the embedded fibers. Irregular surface topography after the first embedded layer produces areas of zero bonding on subsequent layers. This can develop into a vicious cycle which must be avoided to produce a successful build. Using the techniques developed in Section 2.5, an attempt at stacking layers of CF bidirectional fabric was made, with the goal of creating the build described with 6 layers of embedded fabric. However, due to very poor bonding in areas over the channels, pictured in Figure 4.1, not all of the layers were embedded. Figure 4.2 shows a build with two layers of embedded CF fabric. This build suffered delamination due to poor inter-laminate bonding over the fiber channels. The delamination occurred during a machining operation in an effort to level the uneven surface caused by the embedded fibers with deep channels.

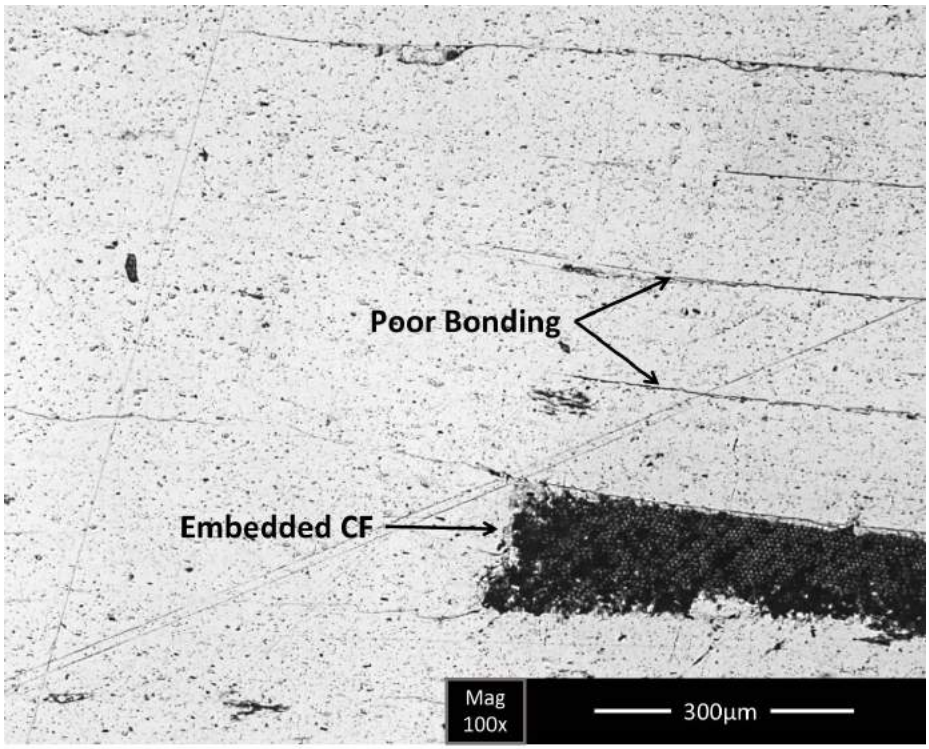

Figure 4.1: Poor bonding with LWD of near zero in the region above embedded CF.

Figure 4.2: Delamination due to poor bonding over embedded channels. Delamination occurred during a machining operation.

4.2 Proposed Joint Design

The root cause of poor inter-laminate bonding leading to delamination is the mechanical mismatch between the height of the CF and the depth of the channels. The aluminum tape deforms into the channels until the majority of the weld force is supported by the material on either side of the channels. Consequently, the weld force on the aluminum tape above the channels is not great enough to induce the shearing forces necessary to form a quality bond. The solution of this issue is to reduce the channel depth to match the height of the carbon fibers. However, doing so while using the current aluminum tape of thickness 0.15 mm, causes severe tearing in the tape over the channels.

The proposed solution which will create an even compliance throughout the weld length and eliminate any tape tearing is to reduce the channel depth as discussed

and use a thicker tape that will not tear over the channels. Ideally the tape thickness would be great enough that only one layer would be welded between each embedded CF fabric. This would greatly reduce manufacturing time. The compliance model discussed in Section 3.2 will be used throughout the design process to better understand the implications of various channel depths while using the thicker tape. Figure 4.3 shows a schematic of the proposed joint geometry. This design features six layers of embedded CF fabric which are stacked directly on top of the previous fabrics. In this manner, maximum strength is achieved by preserving continuous aluminum pillars throughout the joint thickness.

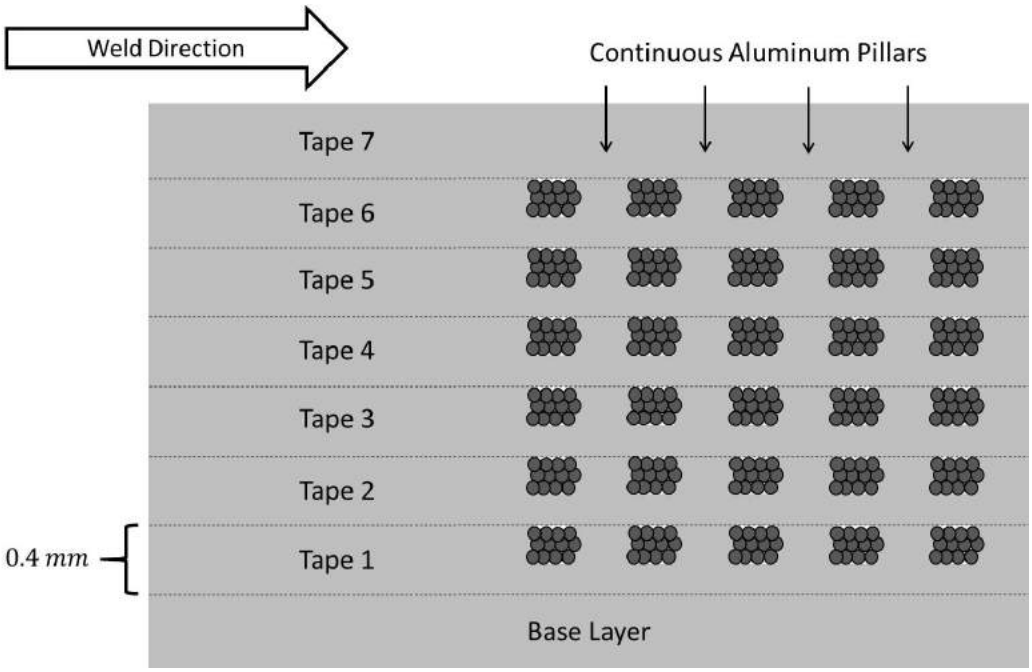

Figure 4.3: Proposed joint with increased tape thickness and reduced channel depth.

One important consequence of using thicker aluminum tape is that the power going into these welds will need to be greater to produce quality inter-laminate bonding. This should not be troublesome since the UAM system used is capable of greater amplitudes than were used for the joint manufacture discussed in Chapter 2. Another potential concern with this design is damage to the carbon fibers during welding. The CF may have a tendency to shear at the tape edge as previously seen in Figures 2.3 and 2.4. The reason for this possibility of fiber damage is due to the fibers supporting most of the weld force with this design. While this may be a real issues with this proposed design, precise adjustments of channel depth, tape thickness and weld parameters, will likely yield a joint with greater strength than adhesive joining.

CHAPTER 5

CONCLUDING REMARKS

5.1 Summary

In this research project, it was shown that carbon fibers can be embedded within aluminum using the UAM process. Furthermore, with the aid of channels for housing, successful consolidation was achieved without damage occurring in the fibers. SEM images verified that the embedded fibers were not crushed. The channels also eliminated any shearing of the fibers at the weld line edge. The result was a CF to aluminum joint formed by mechanical interlocking between the fibers and aluminum.

Mechanical tensile testing on the dry embedded fibers showed that the while the joints had sufficient strength for handling, the joint strength was weak. This was the case because of an uneven load distribution between the fibers. Only the fibers on the perimeter of the embedded bundles carried load, causing them to fail and the fibers on the interior to pullout. After wetting the joints with epoxy, the pullout strength increased by an order of magnitude. One of the joints tested failed in the gauge length of the fiber bundle rather than at the joint. The increased strength came from a more even load distribution between the fibers due to the inter-fiber bonding of the epoxy. The pullout testing demonstrated that under the correct conditions, the UAM

process can be used to create CF to aluminum joints that exceed the strength of the CF.

Further development of CF to aluminum joints was accomplished by embedding full density bidirectional CF fabric within aluminum. Successfully embedding the full density of fibers was troublesome due to tape tearing over the channels orthogonal to the weld direction. However, after selecting proper welding parameters and adjusting the UAM controller gain, successful consolidation was achieved of one layer of CF bidirectional fabric.

Attempts to embed multiple layers of CF fabric exhibited poor inter-laminate bonding over the channels. The inferior quality of the inter-laminate bonding in regions over the channels occurred because of uneven substrate compliance. After tape yielding in these areas, an irregular welding surface was produced. The root cause of the uneven compliance and weld surface was the mismatch between the depth of the channels and the height of the CF being embedded.

The ability to stack successive layers of embedded bidirectional CF fabric is essential to developing joints that are compatible with industry applications. To accomplish this, a joint design featuring thicker aluminum tape was proposed. The thicker tape would eliminate tape tearing and allow for channel depth to be reduced to the height of the fibers, thereby enabling even compliance and producing a more level substrate.

5.2 Future Work

The first item of future work is developing the proposed joint from Chapter 4 to accommodate embedding of a 6-ply carbon fiber composite. This design would utilize the thicker aluminum tape described earlier. To aid in this design process, the compliance model described in Section 3.2 will be used to help minimize variation in the compliance throughout the structure. Speaking in concrete terms, the depth of the channels and other geometric design elements will be based off of this model.

Secondly, once this build is created, it will be mechanically tested in tension. The strength of the joint will then be compared to that of similarly sized adhesive double and single lap joints. This comparison will be a basis of whether the UAM joint is a clear improvement over adhesive methods or not. In order to create a useful comparison, careful test design protocol must be developed and followed. The test design protocol will include (but not be limited by) the following considerations:

- Specimen dimensions
- CF orientation
- Adhesive joint surface finish
- Adhesive joint type: double lap, single lap, or both
- Number of specimens to test: UAM and adhesive
- Additional testing considerations: three-point bending and shear

These decisions will be made based off of ASTM standards when possible. The second point, CF orientation, could influence the structure compliance during the embedding

process. The compliance model from Section 3.2 will be used in the design process for using non-parallel CF orientations.

Third, work must be done to better understand the degree that epoxy is able to impregnate the embedded fibers. This is an important point because as was shown in Section 2.3, the strength of UAM constructed CF to aluminum joints depends on epoxy to create load sharing among the embedded fibers. To insure that the fibers are thoroughly impregnated with epoxy, it may be beneficial to experiment with injecting epoxy prior to consolidating the CF. Another variation of this concept could involve embedding pre-preg CF.

Fourth is the issue of metal matrix material. All the welding performed in this project have been with 6061-T6 H18 aluminum. The most promising applications in the automotive industry involve joining carbon fiber composites to steel. To accommodate this, the principles used in this project would need to be transferred to use with steel as the welding material. The techniques discussed in Chapter 3 will be used to model the compliance of the steel/CF structure. This will act as a basis for steel/CF joint design.

Finally is the issue of corrosion. When dissimilar materials are joined, galvanic corrosion is often a concern, depending on the cathodic or anodic nature of the materials. Carbon fiber is a fairly noble (cathodic) material. Aluminum and steel on the other hand are far more active, making them conducive to corrosion when in direct contact with graphite [28]. This is one area where adhesive joining of CF to metals is superior to other joining techniques. The epoxy used to join the materials also acts as a buffer, preventing galvanic corrosion. While corrosion is a real issue, there may be methods to greatly reduce or eliminate corrosion of UAM joints. Depending on

the application, one solution would be to change the welding metal to stainless steel or titanium. Another could be to completely seal the joined CF structure to avoid contact with any electrolyte fluid. In any case, galvanic corrosion between dissimilar materials is a real issue and will need to be addressed in future research.

BIBLIOGRAPHY

[1] Astm d3528: Standard test method for strength properties of double lap shear adhesive joints by tension loading.

[2] CS Adderley. Adhesive bonding. *Materials & Design*, 9(5):287–293, 1988.

[3] ST Amancio-Filho, C Bueno, JF Dos Santos, N Huber, and E Hage Jr. On the feasibility of friction spot joining in magnesium/fiber-reinforced polymer composite hybrid structures. *Materials Science and Engineering: A*, 528(10):3841–3848, 2011.

[4] F Balle, G Wagner, and D Eifler. Ultrasonic spot welding of aluminum sheet/carbon fiber reinforced polymer–joints. *Materialwissenschaft und Werkstofftechnik*, 38(11):934–938, 2007.

[5] Frank Balle. Joining of dissimilar materials by ultrasonic metal welding. In Khoo Boo Cheong Gan Woon Stong, Lim Slak Plang, editor, *Proceeding of the 2013 International Congress on Ultrasonics*, 2013.

[6] Frank Balle, Stefan Emrich, Guntram Wagner, Dietmar Eifler, Alexander Brodyanski, and Michael Kopnarski. Improvement of ultrasonically welded aluminum/carbon fiber reinforced polymer-joints by surface technology and high resolution analysis. *Advanced Engineering Materials*, 2013.

[7] Frank Balle, Guntram Wagner, and Dietmar Eifler. Ultrasonic metal welding of aluminium sheets to carbon fibre reinforced thermoplastic composites. *Advanced Engineering Materials*, 11(1-2):35–39, 2009.

[8] TA Barnes and IR Pashby. Joining techniques for aluminium spaceframes used in automobiles: Part iiadhesive bonding and mechanical fasteners. *Journal of Materials Processing Technology*, 99(1):72–79, 2000.

[9] Ferdinand P. Beer, Jr E. Russell Johnston, and John T. DeWolf. *Mechanics of Materials (In SI Units) (Mechanical Engineering Series)*. McGraw Hill, 2005.

[10] Ross J Friel, Kenneth E Johnson, Phill M Dickens, and Russell A Harris. The effect of interface topography for ultrasonic consolidation of aluminium. *Materials Science and Engineering: A*, 527(16):4474–4483, 2010.

[11] Hannes Fuchs and Bryan Conrod. Super lap shear joint structural test-analysis correlation studies. In *Society of Plastics Engineers Automotive Composites Conference and Exhibition, Troy MI*, 2010.

[12] LDR Grant, RD Adams, and Lucas FM da Silva. Experimental and numerical analysis of single-lap joints for the automotive industry. *International Journal of Adhesion and Adhesives*, 29(4):405–413, 2009.

[13] Justin Hale. Boeing 787 from the ground up. *Aero Quarterly, Boeing. com Commercial Aeromagazine*, 4:17–23, 2006.

[14] Adam Hehr, Joshua Pritchard, and Marcelo J Dapino. Interfacial shear strength estimates of niti-aluminum matrix composites fabricated via ultrasonic additive manufacturing. In *SPIE Smart Structures and Materials+ Nondestructive Evaluation and Health Monitoring*, pages 905906–905906. International Society for Optics and Photonics, 2014.

[15] CD Hopkins, PJ Wolcott, MJ Dapino, AG Truog, SS Babu, and SA Fernandez. Optimizing ultrasonic additive manufactured al 3003 properties with statistical modeling. *Journal of Engineering Materials and Technology*, 134(1):011004, 2012.

[16] Xiaosong Huang. Fabrication and properties of carbon fibers. *Materials*, 2(4):2369–2403, 2009.

[17] Gordon Kelly. Joining of carbon fibre reinforced plastics for automotive applications. 2004.

[18] Ronald J Kerans and Triplicane A Parthasarathy. Theoretical analysis of the fiber pullout and pushout tests. *Journal of the American Ceramic Society*, 74(7):1585–1596, 1991.

[19] CY Kong, RC Soar, and PM Dickens. Characterisation of aluminium alloy 6061 for the ultrasonic consolidation process. *Materials Science and Engineering: A*, 363(1):99–106, 2003.

[20] CY Kong, RC Soar, and PM Dickens. Optimum process parameters for ultrasonic consolidation of 3003 aluminium. *Journal of materials processing technology*, 146(2):181–187, 2004.

[21] JO Obielodan, A Ceylan, LE Murr, and BE Stucker. Multi-material bonding in ultrasonic consolidation. *Rapid prototyping journal*, 16(3):180–188, 2010.

[22] GD Janaki Ram, C Robinson, Y Yang, and BE Stucker. Use of ultrasonic consolidation for fabrication of multi-material structures. *Rapid Prototyping Journal*, 13(4):226–235, 2007.

[23] Chris Reiter. Bmw makes lone shift to carbon fiber to gain auto edge. *Bloomberg*, 2013.

[24] Eric J Siggard. *Investigative Research Into the Structural Embedding of Electrical and Mechanical Systems Using Ultrasonic Consolidation (UC)*. ProQuest, 2007.

[25] Richard Stewart. Carbon fibre composites poised for dramatic growth. *Reinforced Plastics*, 53(4):16–21, 2009.

[26] S Ucsnik, M Scheerer, S Zaremba, and DH Pahr. Experimental investigation of a novel hybrid metal–composite joining technology. *Composites Part A: Applied Science and Manufacturing*, 41(3):369–374, 2010.

[27] Kunio Uehara and Mitsuru Sakurai. Bonding strength of adhesives and surface roughness of joined parts. *Journal of materials processing technology*, 127(2):178–181, 2002.

[28] Herbert Henry Uhlig and R Winston Revie. *Uhlig's corrosion handbook*, volume 51. John Wiley & Sons, 2011.

[29] Winona State University. Resin transfer molding. course1.winona.edu/kdennehy/ENGR390/Topics/rtm.pptx.

[30] Austin Weber. Composite joining: Adhesive pros and cons. *Assembly Magazine*, 2013. http://www.assemblymag.com/articles/91199-composite-joining-adhesive-pros-and-cons.

[31] Stewart Williams. Joining of dissimilar materials - problems and solutions. http://www.jwi.hw.ac.uk/documents/Willliams$_1$20626$_P$*resn.pdf*.

[32] Paul J Wolcott, Adam Hehr, and Marcelo J Dapino. Optimal welding parameters for very high power ultrasonic additive manufacturing of smart structures with aluminum 6061 matrix. In *SPIE Smart Structures and Materials+ Nondestructive Evaluation and Health Monitoring*, pages 905908–905908. International Society for Optics and Photonics, 2014.

[33] Chunbo Sam Zhang, Andrew Deceuster, and Leijun Li. A method for bond strength evaluation for laminated structures with application to ultrasonic consolidation. *Journal of materials engineering and performance*, 18(8):1124–1132, 2009.